LBL-16162
Preprint c.2

Lawrence Berkeley Laboratory
UNIVERSITY OF CALIFORNIA

Materials & Molecular Research Division

RECEIVED
LAWRENCE
BERKELEY LABORATORY
AUG 29 1983
LIBRARY AND
DOCUMENTS SECTION

Submitted to Metallurgical Transactions

SOURCES OF INTERGRANULAR EMBRITTLEMENT DURING HIGH TEMPERATURE TESTING OF AN IRON BASE SUPERALLOY

G.-X. Hu and J.W. Morris, Jr.

August 1982

TWO-WEEK LOAN COPY
This is a Library Circulating Copy which may be borrowed for two weeks. For a personal retention copy, call Tech. Info. Division, Ext. 6782.

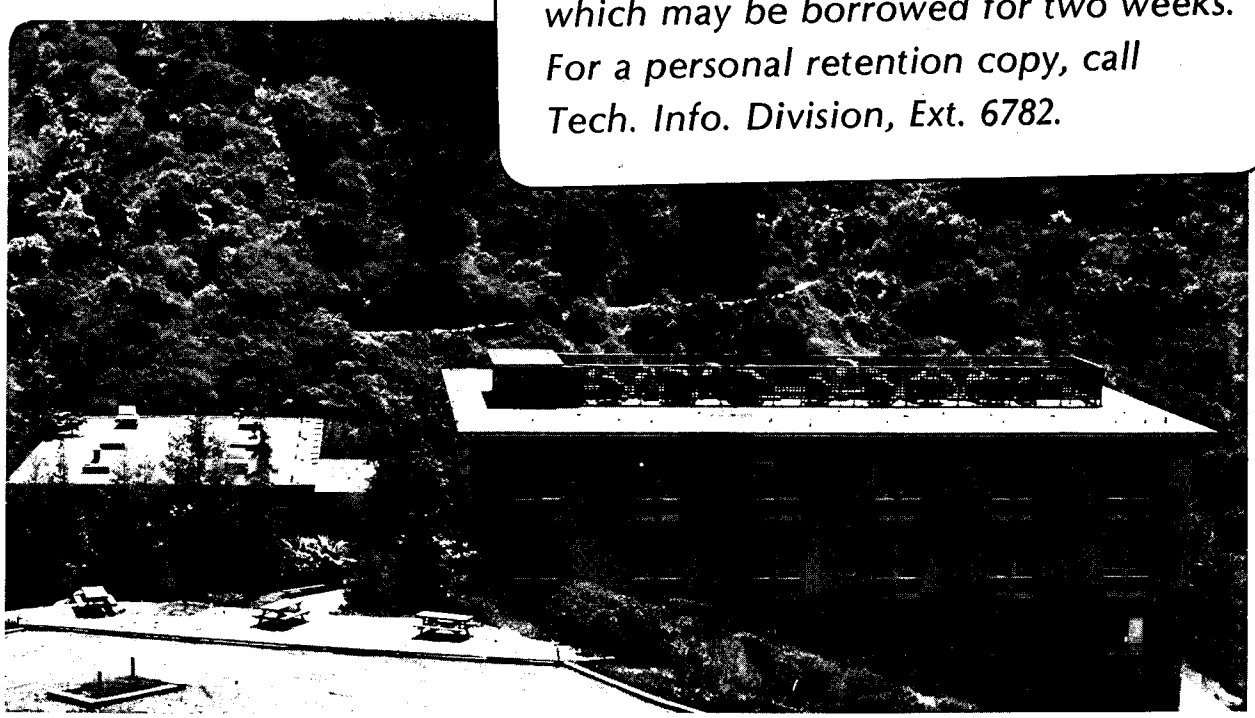

LBL-16162 c.2

Prepared for the U.S. Department of Energy under Contract DE-AC03-76SF00098

DISCLAIMER

This document was prepared as an account of work sponsored by the United States Government. While this document is believed to contain correct information, neither the United States Government nor any agency thereof, nor the Regents of the University of California, nor any of their employees, makes any warranty, express or implied, or assumes any legal responsibility for the accuracy, completeness, or usefulness of any information, apparatus, product, or process disclosed, or represents that its use would not infringe privately owned rights. Reference herein to any specific commercial product, process, or service by its trade name, trademark, manufacturer, or otherwise, does not necessarily constitute or imply its endorsement, recommendation, or favoring by the United States Government or any agency thereof, or the Regents of the University of California. The views and opinions of authors expressed herein do not necessarily state or reflect those of the United States Government or any agency thereof or the Regents of the University of California.

SOURCES OF INTERGRANULAR EMBRITTLEMENT DURING HIGH TEMPERATURE TESTING OF AN IRON BASE SUPERALLOY

G.-Xiang Hu* and J. W. Morris, Jr.

Department of Materials Science and Mineral Engineering
University of California
and
Materials and Molecular Research Division
Lawrence Berkeley Laboratory

ABSTRACT

This work was undertaken to investigate the elevated temperature tensile properties of a new age-hardened iron-based superalloy, EPRI-T (Fe-34.5Ni-5Cr-3Ti-3Ta-1Mo-0.01B), that was designed to combine high strength and good fracture toughness at room temperature. The alloy retained high strength when tested at 650°C in air. However, samples that were aged from the annealed condition were brittle at 650°C. Fractographic analyses of the embrittled specimens showed that they failed in an intergranular mode that initiated at the sample surface. Samples cut longitudinally from material that was aged directly from the as-forged condition were ductile in tension at 650°C. The intergranular surface cracks could not penetrate the elongated grains parallel to the tensile axis. The weakness of the grain boundaries was found to be due to cellular precipitation of the Fe_2Ta Laves phase. An alternate heat treatment was designed to suppress cellular precipitation. Samples given this heat treatment had improved room temperature ductility and remained ductile when tested at 650°C in vacuum, but were brittle when tested in 650°C air. The high temperature brittleness is caused by subsurface oxidation, which induces precipitation of the Laves phase along the grain boundaries ahead of the growing oxide. Hence the alloy embrittles itself when tested at a low strain rate in high temperature air. A parallel investigation studied the influence of mechanical twinning on the high temperature deformation of the alloy. Twinning occurs, but appears to be a consequence of the embrittling mechanism rather than a cause of embrittlement.

*Present Address: Jaio-Tong University, Shanghai, People's Republic of China

INTRODUCTION

Many austenitic steels and nickel-based alloys exhibit a rapid drop in tensile ductility when tested in air in the intermediate temperature range 600-750°C [1-4]. The decrease in ductility is associated with a change in the fracture mode from transgranular to intergranular failure. The intergranular fracture was originally suggested [3,4] to result from cavitation due to restrictions on grain boundary sliding. However, more recent work [5-11] has shown that the embrittlement usually disappears when the testing is carried out in inert environments, which implicates oxygen as the embrittling species. Oxygen diffuses along the grain boundaries and may plausibly lead to embrittlement by grain boundary pinning [8] or, in superalloys, by interaction with a grain boundary [6] or matrix [5] precipitate phase. The experiments that document the oxygen effect were, however, done on specimens that had been exposed to high temperature air for extensive periods prior to testing. It is not clear whether oxygen embrittlement also influences the high temperature ductility of fresh specimens.

An alternate theory [12] attributes the ductility minimum to mechanical twinning during elevated temperature tests. In this interpretation the impingement of twins on the grain boundary causes high stress concentrations that are relieved by grain boundary cracking. But the researchers who proposed this mechanism obtained different results with another superalloy; in this case they suggested that twin nucleation relieved stress concentrations at the grain boundaries. The role of twinning needs further clarification.

The present research was undertaken to study the high temperature tensile behavior of a high strength iron-based superalloy, designated EPRI-T [13-15], which was developed for potential use near room temperature in the retaining rings of large electrical generators. The alloy has a nominal composition, in wt.%, Fe-34.5Ni-3Ti-3Ta-0.5Al-1Mo-0.3V-0.01B, and employs Ti and Ta as major γ' precipitation strengtheners. It develops a room temperature yield strength above 1380 MPa (200 ksi) with a fracture toughness in excess of 110 $MPa \cdot m^{1/2}$ (100 $ksi \cdot in^{1/2}$) after double aging from as-forged condition, and also has good properties, with slightly lower strength, when aged after an intermediate solution anneal. Because of its exceptional combination of strength and toughness at room temperature, the elevated temperature properties of the alloy were of interest. The experiments reported below show that the alloy retains excellent strength at temperatures up to 650°C, but is susceptible to high temperature embrittlement when tested in air. The mechanism of high temperature embrittlement was studied in some detail to clarify the behavior of this particular alloy, to identify metallurgical techniques for controlling high temperature embrittlement, and to gain further insight into the mechanisms of high temperature embrittlement in iron-based superalloys.

EXPERIMENTAL PROCEDURE

The nominal chemical composition of EPRI-T and the analyzed composition of the alloy used for these tests are given in Table 1. The experimental specimens were cut from 30mm thick by 70mm wide forged

barstock. They were heat treated before machining. The 'as-rolled' condition was established by rolling square sections cut from the forged billet from 30mm to 15mm thickness at 1100°C and water quenching.

Tensile tests were performed at room temperature and at elevated temperature. The elevated temperature tests were done in two different environments. The first was low pressure air maintained by evacuating the heating tube with a mechanical pump to about 70-100 μm Hg. The specimen surfaces inevitably turned dark after testing at 650°C, indicating surface oxidation. A second series of tests were conducted in a vacuum of 1×10^{-4} torr. In this case the specimen surfaces remained bright after the test. The tensile specimens tested at room temperature and at elevated temperature in air had a gage diameter of 6.35mm and a reduced section of 31.7mm. The specimens tested in vacuum had a 4.06mm gage diameter and a 26mm reduced section. A crosshead speed of 0.5mm/min was used for all tensile tests, yielding a nominal strain rate of about 0.017 min^{-1}.

Optical and scanning electron microscopy (SEM) were used to examine metallographic samples, including the fracture surfaces of the failed tensile specimens. Transmission electron microscopic (TEM) studies were done on thin foil specimens cut from heat treated samples or from the gage length of tested tension specimens. Chemical microanalysis was done with energy dispersive spectrometry (EDS) in the SEM or scanning transmission electron microscope (STEM) and by Auger Electron Spectroscopy (AES). The etchant used for metallographic samples contained of 15ml HNO_3, 5ml HF and 200ml H_2O. The jet polishing solution for preparing thin foils was made from 75g CrO_3, 400ml CH_3OOH, and 21ml H_2O.

RESULTS AND DISCUSSION

1. Tensile Tests in Air.

The temperature 650°C was chosen for the elevated temperature tensile tests for two reasons. First, the alloy overages in a relatively short time at temperatures above 650°C, so this is its maximum working temperature. Second, iron-based superalloys typically exhibit a severe embrittlement when tested in air at 650°C, so this is a useful temperature at which to test its propensity to embrittle. The first set of tensile tests was done at room temperature and at 650°C, using samples in two heat treatment conditions [15]: (1) 'as-rolled' + 750°C/4H + 670°C/6H ('as-rolled' samples); (2) 970°c/1.5H, water quench, + 750°C/4H + 670°C/6H ('solution treated' samples). The results are the first two data sets listed in Table 2.

Both sets of specimens maintained high strength when tested at 650°C in air. However, the two sets differed dramatically in ductility and fracture behavior. The 'as-rolled' specimens fractured in a ductile mode, and had higher elongation and reduction in area at 650°C than they had at room temperature (Fig. 1a). The 'solution treated' specimens, on the other hand, embrittled seriously at 650°C and had prominent surface cracks after testing (Fig. 1b). Fractographic analyses revealed a band of intergranular fracture around the specimen surface which extended inward to a depth of about one-third of the sample radius (Fig. 2a).

The fracture then changed to a predominantly transgranular mode in the sample center (Fig. 2b). This observation, coupled with the extensive surface cracking observed on the remainder of the specimen surface, showed that fracture began at grain boundaries on the exposed surface and propagated inward along the grain boundaries until reaching critical size.

2. Microstructural Interpretation of the Test Results.

A microstructural analysis was performed to determine the metallurgical source of the different behavior of these specimens.

a. The 'Solution-Treated' Specimens. Metallographic studies of the 'solution-treated' samples revealed a fine, cellular precipitation along the grain boundaries. The cellular precipitates appear in suitably etched metallographic samples (Fig. 3a) and are evident in thin foil samples examined by TEM (Figs. 3b, 3c). The detrimental effect of cellular precipitation on the ductility of superalloys is well known [16-18]. The cellular precipitates have two negative effects: they inhibit slip deformation and they crack, initiating fracture.

The metallographic data show that cellular precipitates are present in the initial specimens, and that further precipitation occurs dynamically during testing. Specimens cut from the fractured samples have a perceptibly higher density of cellular precipitates than is present before testing. The strain-induced precipitation is illustrated in Figure 4. In this micrograph, which was taken from near the center of a tension specimen, cellular precipitates decorate both the grain boundaries and the slip bands in the grain interior. The micrograph also illustrates intergranular cracking in the specimen interior, and suggests its mechanism. The internal cracks apparently begin as cavities or microcracks at weak interfaces, and grow or propagate until they link together. The specific association of cellular precipitation and intergranular fracture is also apparent from SEM micrographs of the material near the fracture surface, such as that presented in Fig. 5.

The metallographic data also suggest that oxidation contributes to the high temperature brittleness of the alloy. In contrast to normal tensile behavior, in which fracture originates from the center of the sample, the critical intergranular cracks begin from the sample surface. Intergranular surface cracks were even occasionally found at the curved fillet of the failed specimen (Fig. 6) where the applied stress was less than in the gage section. There is an oxidized layer of about 1-2 μm thickness on the specimen surface; the depth of oxygen penetration along the grain boundaries must be much greater. It hence appears that the intergranular embrittlement is due to the combined effects of cellular precipitation and oxygen.

b. The 'As-rolled' Specimens. The microstructure of a longitudinal section of the the as-rolled and double-aged specimen is illustrated in Figure 7. The grains are elongated in the rolling direction, showing that the alloy did not recrystallize during rolling. Transmission electron microscopy reveals a polygonized substructure. Grain boundary precipitates are also present when the alloy is in this condition (Fig. 8), but they are smaller than in the 'solution-treated' specimens and

are blocky in shape. The change in precipitate morphology is presumably due to the substructure, which introduces a high density of nucleation sites within the grains.

The excellent high temperature ductility of the 'as-rolled' specimens is apparently due to their orientation, which places the long axes of the elongated grains parallel to the sample axis. As shown in Figure 9, surface cracks develop along the grain boundaries that are normal to the tensile axis, but propagate only a short distance before being stopped at perpendicular grain boundaries. Hence the specimens fail in a ductile mode.

The ductility of the 'as-rolled' alloy is metallurgically interesting, and may be useful in certain applications, but is limited to load geometries in which the tensile axis is nearly parallel to the long axis of the grains.

3. Design of a Heat Treatment to Suppress Cellular Precipitation.

There appear to be two factors that contribute to high temperature embrittlement: cellular precipitation and oxygen attack. One of these, cellular precipitation, is a metallurgical phenomenon that may plausibly be eliminated by proper processing.

a. Characteristics of the Cellular Precipitation. To eliminate the intergranular precipitate it is necessary to identify it. A number of intermetallic phases precipitate from iron-based superalloys, including the $\eta(Ni_3Ti)$, $\delta(Ni_3Nb)$, Laves, σ, and μ phases. The composition of this particular alloy permits either the η phase, Ni_3Ti, or the Laves phase, Fe_2Ta, of type $MgZn_2$. Because both of these phases have hexagonal structures, they are difficult to distinguish by x-ray or electron diffraction. But they are significantly different in chemical composition. The η phase is nearly stoichiometric [19,20] and does not readily accept substitutional impurities. The $MgZn_2$-type Laves phase, on the other hand, has the general formula $(Fe, Mn, Cr,Si)_2(Mo,Ti,Nb,Ta)$ [18]. It contains little or no nickel, and should, therefore, be distinguishable from the η-phase on the basis of its composition.

Energy dispersive x-ray microanalysis (EDS) was performed in a scanning transmission electron microscope (STEM) to determine the composition of the cellular precipitate. A typical result is given in Figure 10. The x-ray spectra show that the precipitate is rich in Ta, Mo and Ti relative to the γ matrix, but is much lower in Ni. It appears to be the Laves phase. This identification is consistent with the thermodynamics of the alloy. The solubility of Ta in iron is very low [21], approximately 0.5 atom percent at 1293°C and 0.3 at 974°C. The Laves phase forms at higher Ta contents. Moreover, Ti and Mo are Laves-forming elements. It is, hence, reasonable that the Laves phase should form in preference to the η phase.

The temperature range of cellular precipitation was studied by isothermally aging solution-treated samples in the range 650°C to 950°C at 50°C intervals. Cellular precipitation was not observed until the aging temperature reached 750°C. The kinetics of precipitation then increased with the aging temperature. Cellular precipitation was most

pronounced in the range 850-900°C, but persisted at 950°C before disappearing at 1000°C.

The precipitate morphology is illustrated in Figure 11. The cellular grain boundary precipitates can be seen clearly, and grow from one grain into another. It is interesting that the precipitate morphology does not change significantly with the reaction temperature. Figure 12, for example, shows cellular precipitates formed at 950°C; they closely resemble the precipitates in samples aged at lower temperatures. This behavior contrasts with that typical of the cellular precipitation of the η or carbide phases, which tend to change to a Widmanstatten pattern within the grains [18,21] or a globular form in the grain boundaries [16] at higher temperature.

b. Suppression of the Cellular Precipitation. The heat treatment originally given this alloy, double-aging at 750°C and 670°C, was intended [13-15] to establish a dense distribution of fine intragranular γ' precipitates in a reasonable aging time, so that the alloy would have a good combination of room temperature mechanical properties. The observations reported above show that cellular precipitation inevitably occurs during the 750°C step. However, the principal purpose of the 750°C aging was to increase the initial precipitation rate so that the total aging time would not be excessive. The alloy properties do not depend on starting the heat treatment at 750°C.

We therefore attempted to suppress cellular precipitation by adding a preliminary aging treatment at a temperature below 700°C. The purpose of the preliminary aging was to initiate intragranular precipitation of the γ' phase and decrease the Ta supersaturation, hence lowering the driving force for cellular precipitation during subsequent aging at 750°C. A preliminary age at 680°C for 16 hours appears to be sufficient. If the alloy is subsequently given the usual double aging treatment it achieves the same high strength level (Table 2), but no cellular precipitates are found.

Alloy specimens that were double-aged with and without the preliminary aging treatment were tested in tension at room temperature and at 650°C in air. The results are presented in Table 2. The triply-aged specimens were somewhat more ductile at room temperature, and seemed to offer a slight improvement at 650°C. But they were still brittle at 650°C, and still fractured in an intergranular mode. Post-failure analysis of the triply-aged specimens showed the expected surface oxidation (Fig. 13), but also revealed cellular precipitates along the grain boundaries ahead of the intergranular cracks that had propagated in from the specimen surface (indicated by arrows in Figure 13). These intergranular precipitates were not present in the sample before testing, and hence must have formed during the test. It was not clear whether they were caused by the stress at high temperature or by the exposure to oxygen.

4. Tensile Tests in Vacuum.

To separate the influence of stress at high temperature from the effect of the oxygen environment triply-aged specimens were tested in a vacuum of 10^{-4} torr. Examples of the results are presented in Figure 14

and in Table 3, and are compared to the results of similar tests in air.

The triply-aged specimens were ductile at high temperature in vacuum. The specimen tested at 650°C in vacuum had a reduction in area at fracture that was twice the value of a similar specimen tested in air at 650°C, and was almost equal to the room temperature value (Fig. 3). The ductility of the specimens in vacuum decreased slightly with temperature (quite possibly because of the residual partial pressure of oxygen in the chamber [8]), but the decrease was minor compared to that in similar specimens tested in air. The specimens that were tested in vacuum invariably broke in a normal cup-and-cone fracture. The failure initiated in the center of the specimen and propagated in a transgranular, ductile mode (Fig. 15). The specimens necked appreciably prior to fracture. No intergranular surface cracks were found.

These results led us to conclude that the high temperature embrittlement of the alloy is primarily due to oxygen.

5. The Mechanism of Oxygen Embrittlement.

Several mechanisms have been proposed to explain high temperature oxygen embrittlement. These include oxide wedging due to accelerated grain boundary oxidation in the applied stress field [22], dynamic interaction between oxygen and the γ' precipitates on the grain boundary [6], and grain boundary pinning by oxygen [8,10]. But the most striking feature of the embrittled specimens tested in this work was the association between the oxide-induced surface cracking and the cellular precipitation. We were particularly struck by the appearance of cellular precipitates on and ahead of the intergranular surface cracks in triply-aged specimens that had no detectable cellular network prior to testing. We therefore designed and conducted experiments to test for mechanistic connections between oxidation, surface cracking, and dynamic cellular precipitation.

Samples of the alloy were heated in air at 1100°C for two hours, water quenched, and then aged at 750°C for 8 hours. An external oxide scale formed during initial heating at 1100°C, but spalled away on cooling, leaving the gross internal oxide layer shown in Figure 16a. During the subsequent aging at 750°C a zone of extensive cellular precipitation formed beneath the oxide layer, as shown in Figure 16b. This subsurface cellular precipitation was evidently an environmental effect since cellular precipitates were rarely found in the interior of the specimen.

To identify the cause of the subsurface cellular precipitation Auger electron spectroscopy (AES) was used to map the composition of the surface region. Typical Auger spectra of the internal oxide layer, the cellular precipitate zone, and the $\gamma + \gamma'$ matrix are given in Figure 17, and the semiquantitative analysis of the data is presented in Table 4. The Auger analysis showed that the internal oxide layer is relatively rich in titanium and nickel and lean in iron and tantalum, while the cellular precipitate zone is rich in Fe and Ta and depleted of Ni and Ti. It hence appears that Ni and Ti migrate preferentially to the oxide, leaving a subsurface layer that is rich in Fe and Ta and causing the cellular precipitation of the Laves phase.

These results, taken together with the results of the high temperature tensile tests, suggest that the present alloy is self-embrittling when tested at high temperature in air. The apparent mechanism of embrittlement is the following.

When the alloy is strained at high temperature in air oxygen attacks the grain boundaries that impinge on the external surface of the sample, forming an oxide that is rich in Ni and Ti and increasing the concentration of Ta in the subsurface layer ahead of the oxide. The combination of high temperature, applied stress, and Ta enrichment causes a rapid intergranular cellular precipitation of the Fe_2Ta Laves phase that locally embrittles the grain boundaries. The embrittlement leads to intergranular fracture, which facilitates oxygen penetration along the grain boundary and promotes further precipitation ahead of the crack tip. The process is repeated until the surface flaws reach critical size and the sample breaks.

This mechanism clearly operates in the particular superalloy studied here and contributes to its high temperature embrittlement. The mechanism may be more generally applicable. Most commercial superalloys are complex alloys that contain several phases and are liable to form deleterious grain boundary precipitates under appropriate conditions. If surface oxidation promotes the precipitation of a brittle grain boundary phase, of whatever specific composition, then the alloy will be self-embrittling at high temperature in air.

6. The Influence of High Temperature Twinning on Ductility.

A subsidiary issue that was also addressed in this research is the influence of mechanical twinning on high temperature embrittlement. Recent investigations have demonstrated that mechanical twinning occurs during high temperature tensile deformation [12,23,24] or fatigue [25,26] in a number of superalloys. It has been suggested [12] that the high temperature ductility minimum is due to twinning, in that the impingement of twins on the grain boundaries cause stress concentrations that are relieved by grain boundary cracking.

To clarify the influence of mechanical twinning on the ductility of the present alloy longitudinal sections were cut from tensile specimens that had been tested to failure at 650°C. Metallographic analysis showed that the dominant mechanism of high temperature deformation was planar slip. The transmission electron micrograph presented in Figure 18, for example, shows planar dislocation arrays on the {111} slip planes that impinge on an annealing twin. Arrays of slip dislocations can also be seen on the other side of the twin on the plane that is the mirror image of the incident slip plane. Mechanical twins are also found; examples are given in Figs. 19 and 20. The latter micrograph shows a slip band crossed by a deformation twin. However, the deformation twins were comparatively rare.

An analysis of the distribution of the deformation twins indicates that these are most common where microstructural obstacles such as cellular precipitates impede dislocation slip. Figure 21, for example, shows deformation twins near a grain boundary that is decorated by

cellular precipitates. Grain boundary cracks were occasionally found in association with mechanical twins, but only when the twin impinged on a decorated boundary. An example is given in Figure 22.

This evidence suggests that mechanical twinning is primarily a consequence of embrittlement rather than its cause. The twins form predominantly in regions of the specimen where precipitation largely prevents slip. There is some associated grain boundary cracking, but it occurs on grain boundaries that are liable to intergranular fracture in any case.

CONCLUSIONS

1. The iron-based superalloy EPRI-T has excellent high temperature strength, but is brittle when tested at temperatures above 650°C in air. The brittle mode is intergranular fracture that initiates from the sample surface during tensile tests.

2. The embrittlement is due to a combination of surface oxidation and intergranular cellular precipitation of the Fe_2Ta Laves phase. The two phenomena are coupled. Oxidation depletes the alloy surface of Ni and Ti, causing an enrichment in Ta and promoting cellular precipitation along the grain boundaries. The alloy is hence self-embrittling when exposed to oxygen at high temperature under stress.

3. A three-step heat treatment, developed in the course of the research, suppresses intergranular cellular precipitation during aging of the alloy. Specimens given this heat treatment have good high temperature ductility when tested in vacuum, but self-embrittle when tested in air.

4. Samples that are aged directly from an as-rolled condition and tested in the longitudinal direction have good high temperature ductility in air. The ductility is a consequence of the grain shape in the sample. Elongated grains, oriented along the tensile axis, prevent the propagation of the intergranular fractures that initiate on the sample surface.

5. The dominant mechanism of high temperature deformation is slip. Mechanical twinning also occurs, but is largely confined to regions of the alloy that are decorated by cellular precipitates. Mechanical twinning is a consequence rather than a cause of embrittlement.

ACKNOWLEDGEMENTS

The authors are grateful to Prof. Y. T. Chou and Dr. W. G. Nachtrad of Lehigh University for making their laboratory and expertise available for the tests at high temperature in vacuum. The authors are also grateful to Dr. K. M. Chang, of the General Electric Research and Development Laboratory, for helpful discussions. This work was supported by the Director, Office of Energy Research, Office of Basic Energy Sciences, Materials Sciences Division of the U. S. Department of Energy under Contract No. DE-AC03-76SF00098.

REFERENCES

1. Newell, H. O.: Book of Stainless Steels, ASM, 1933, p. 364.

2. Betteridge, W.: The Nimonic Alloys, E. Arnold (ed.), London, 1959, p. 142.

3. Rhines, F.N. and Wray, P.J.: Trans. ASM, 1961, vol. 54, p. 117.

4. Sikka, V.K., Swindeman, R.W. and Brinkman, C.R.: Fracture, 1977, vol. 2, p. 561.

5. Prager, M. and Sines, G.: Trans. ASME, 1971, p. 225

6. Chang, W.H.: Superalloys-Processing, Proc. 2nd Int. Conf. on Superalloys, Seven Springs, Section V, AIME, 1972.

7. Woodford, D.A.: Met. Trans. A, 1981, vol. 12A, p. 299.

8. Bricknell, R.H. and Woodford, D.A.: Met. Trans. A, 1981, vol. 12A, p. 425.

9. Woodford, D.A. and Bricknell, R.H.: Met. Trans. A, 1981, vol. 12A, p. 1467.

10. Bricknell, R.H. and Woodford, D.A.: Met. Trans. A, 1981, vol. 12A, p. 1673.

11. Woodford, D.A. and Bricknell, R.H.: Met. Trans. a, 1981, vol. 12A,p. 1945.

12. Remy, L.: Met. Trans A, 1981, vol. 12A, p. 387.

13. Chang, K.M., Morris, Jr., J.W. and Thomas, G.: EPRI CS-1808, Interim Report, April, 1981.

14. Chang, K.M. and Morris, Jr., J.W. : Proc. MICON Symposium, Houston, Texas, January, 1982.

15. Viswanathan, R., Morris, Jr. J.W. and Chang, K. M: J. Mat. Energy Systems, September, 1981, vol. 3, pp. 3-6.

16. Beattie, H.J. and Ver Snyder, F.L.: Trans. ASM, 1957, vol. 49, p. 883.

17. Muzyka, D.R.: in The Superalloys, C.T. Sims and W.C. Hazel (eds.), Wiley, New York, 1972, p. 125.

18. Sullivan, C.P. and Donachie, Jr., M.J.: Metals Eng. Quar., Nov., 1971, p. 1.

19. Taylor, A.: Trans. AIME, vol. 72, 1957, p. 72.

20. Moll, J.H., Maniar, G.N. and Muzyka, D.R.: Met. Trans., 1971, vol. 2, p. 2143.

21. Mihalisen, J.R. and Decker, R.F.: Trans. AIME, vol. 218, 1960, p. 507.

22. Barlon, R. and Grundy, P.J.: J. Mat. Sci., 1969, vol. 4, p. 797.

23. Guimier, A. and Strudel, J.L.: Proc. and Int. Conf. on the Strength of Metals and Alloys, Asilomar, 1970, p. 1145.

24. Chang, K.M.: General Electric Co. Report No. 82 CRD 048, February, 1982.

25. Fournier, D. and Pineau, A.: Met. Trans. A, 1977, vol. 8A, p. 1095.

26. Sanders, Jr., T.H., Frishmuth, R.E. and Embley, G.T.: Met. Trans. A, 1981, vol. 12A, p. 1003.

Table 1. Nominal and Analyzed Composition of the Research Alloy (in weight percent).

Material	EPRI-T Nominal Composition	Analysis of Alloy
C	-	0.007
Fe	Bal.	Bal.
Ni	34.50	35.26
Cr	5.00	4.94
Ti	3.0	3.2
Ta	3.0	3.06
Al	0.5	0.49
Mo	1.0	0.97
V	0.30	0.39
B	0.01	0.008

Table 2. Tensile Properties of Specimens Tested at Room Temperature and at 650°C in Air.

Treatment	0.2 Y.S. (MPa) 20°C	0.2 Y.S. (MPa) 650°C	U.T.S. (MPa) 20°C	U.T.S. (MPa) 650°C	Pct. Elong. 20°C	Pct. Elong. 650°C	Pct. R.A. 20°C	Pct. R.A. 650°C
As-rolled	1420	1096	1502	1227	14	18	48	57
+750°C/4h + 670°C/6h	1344	1061	1517	1151	13	14	39	46
970°C/1.5h W.Q.	1096	910	1448	1075	17	10	38	15
+750°C/4h + 670°C/6h	1068	931	1420	1020	20	10	44	14
1000°C/1.5h W.Q. +	1138	951	1455	1124	23	14	51	24
680°C/16h + 750°C/4h + 670°C/8h		938		1082		14		20

Table 3. Tensile Properties of Specimens Tested at 650°C in Vacuum and in Air (Treatment: 1000°C/1.5h W.Q + 680°C/16h A.C. + 750°C/4h A.C. + 670°C/8h A.C.).

Environment	0.2 Y.S. (MPa)	U.T.S. (MPa)	Pct. Elong.	Pct. R.A.
Vacuum	984	1152	16	47
	962	1120	16	45
Air	951	1124	14	24
	938	1082	14	20

Table 4. AES Semiquantitative Data of Different Zones in a Surface Oxidized Sample (atomic pct).

	Fe	Ni	Cr	Ti	Ta
Internal oxide layer	17.8	64.3	6.3	10.0	1.6
Precipitation zone	59.9	26.7	6.6	3.1	3.7
$\gamma + \gamma'$ matrix	53.6	32.8	5.5	5.8	2.3

FIGURE CAPTIONS

1. Optical macrographs of tensile specimens fractured at 650°C. (a) 'As-rolled' specimen tested in air; (b) 'solution-treated' specimen tested in air; (c) triply-aged specimen tested in vacuum.

2. Scanning electron fractographs of the fracture surface of a 'solution-treated' specimen that was broken in tension at 650°C in air (a) Intergranular fracture near the outer surface; (b) change in the fracture mode near the sample center.

3. Examples of cellular precipitation in a 'solution-treated' specimen. (a) Scanning electron micrograph; (b) and (c) transmission electron micrographs.

4. An optical micrograph illustrating the initiation of intergranular fracture from cavities formed at grain boundaries that are decorated by cellular precipitates.

5. Scanning electron fractograph showing cellular precipitates in the intergranular fracture surface.

6. Optical micrograph showing intergranular surface cracks in the curved fillet region of a 'solution-treated' specimen tested at 650°C in air.

7. Optical micrograph of a longitudinal section of the 'as-rolled' specimen.

8. Transmission electron micrograph of a grain boundary in an 'as-rolled' specimen showing intergranular precipitates.

9. Optical micrograph of a longitudinal section through an 'as-rolled' specimen that was broken in tension at 650°C in air. Intergranular surface cracks are present, but are blunted at the grain boundaries of the elongated grains and remain shallow.

10. STEM-EDS spectra of the intergranular precipitate phase (solid line) and the matrix (dotted line) showing that the precipitate in enriched in Ta and is lean in Ni relative to the matrix.

11. Scanning electron micrograph of cellular precipitates in the boundary of a specimen that was aged at 800°C for 16 hours.

12. Optical micrograph showing cellular precipitates in a specimen that was aged at 940°C for 2 hours.

13. Surface oxidation (bottom) and subsurface intergranular cracks in a specimen that was tested in tension at 650°C in air. The arrows point to intergranular cellular precipitates ahead of the crack tip.

14. The variation of the reduction in area at fracture in tension with testing temperature for triply-aged specimens tested in vacuum (open circles) and air (filled circles).

15. Scanning electron fractograph of the broken surface of a triply-aged specimen that was broken in tension in vacuum at 650°C.

16. Optical micrographs of sections through samples that were oxidized by heating in air at 1000°C for 2 hours. (a) After quenching to room temperature; (b) after subsequent aging at 750°C for 8 hours, showing extensive cellular precipitation through the subsurface region.

17. Auger electron spectra of material near the oxidized surface. (a) The internally oxidized layer; (b) the zone of extensive cellular precipitation; (c) the $\gamma + \gamma'$ matrix.

18. Transmission electron micrograph showing planar dislocation arrays formed during tensile deformation at 650°C.

19. Transmission electron micrograph of a mechanical twin that formed during tensile deformation at 650°C: (a) bright field view; (b) corresponding dark field view.

20. Transmission electron micrograph showing a twin crossing a slip band in a specimen deformed in tension at 650°C: (a) bright field view; (b) corresponding dark field view.

21. Transmission electron micrograph showing twins impinging on a grain boundary that is decorated by cellular precipitates.

22. Optical micrograph showing the initiation of intergranular fracture in a region containing both intergranular cellular precipitates and twins that impinge on the decorated grain boundaries. The latter are indicated by arrows in the figure.

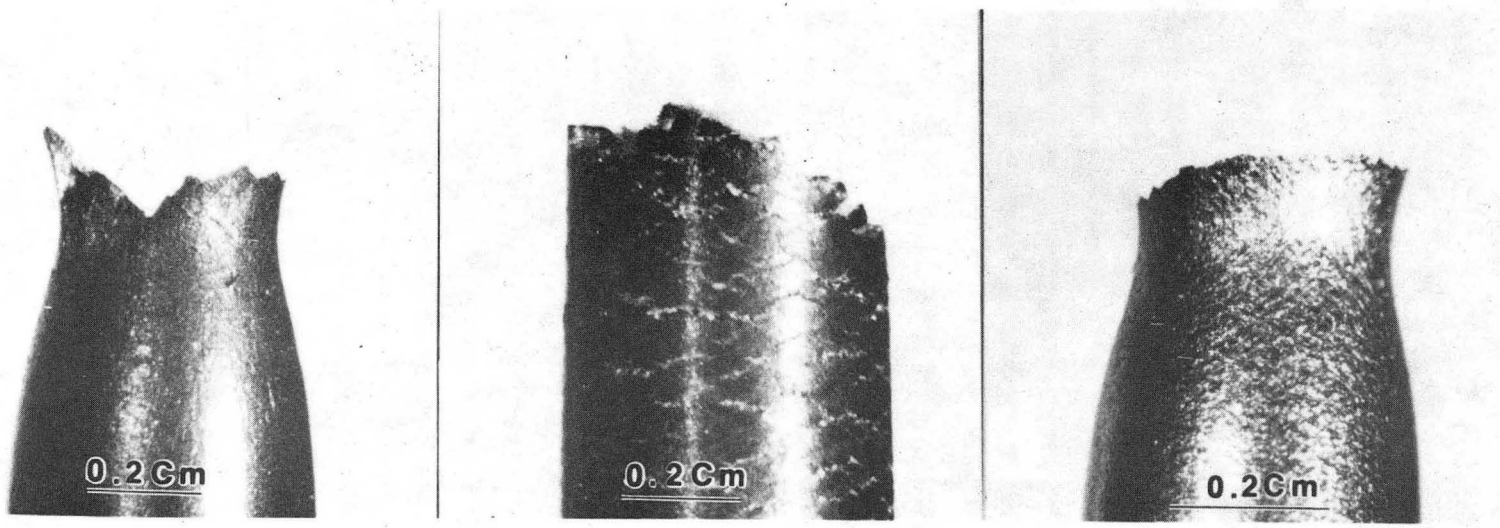

Figure 1

XBB 827-6739

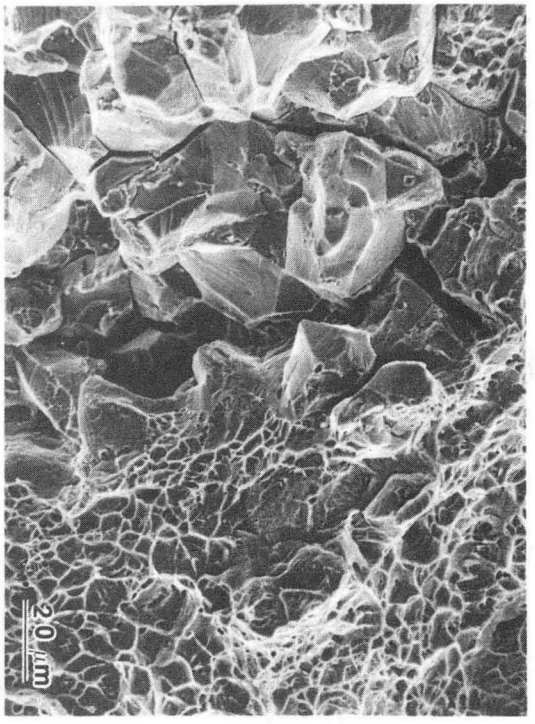

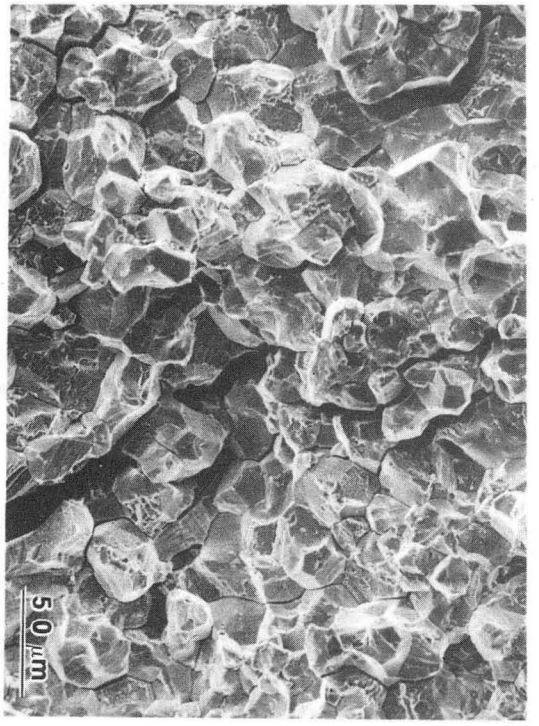

Figure 2

XBB 827-6441

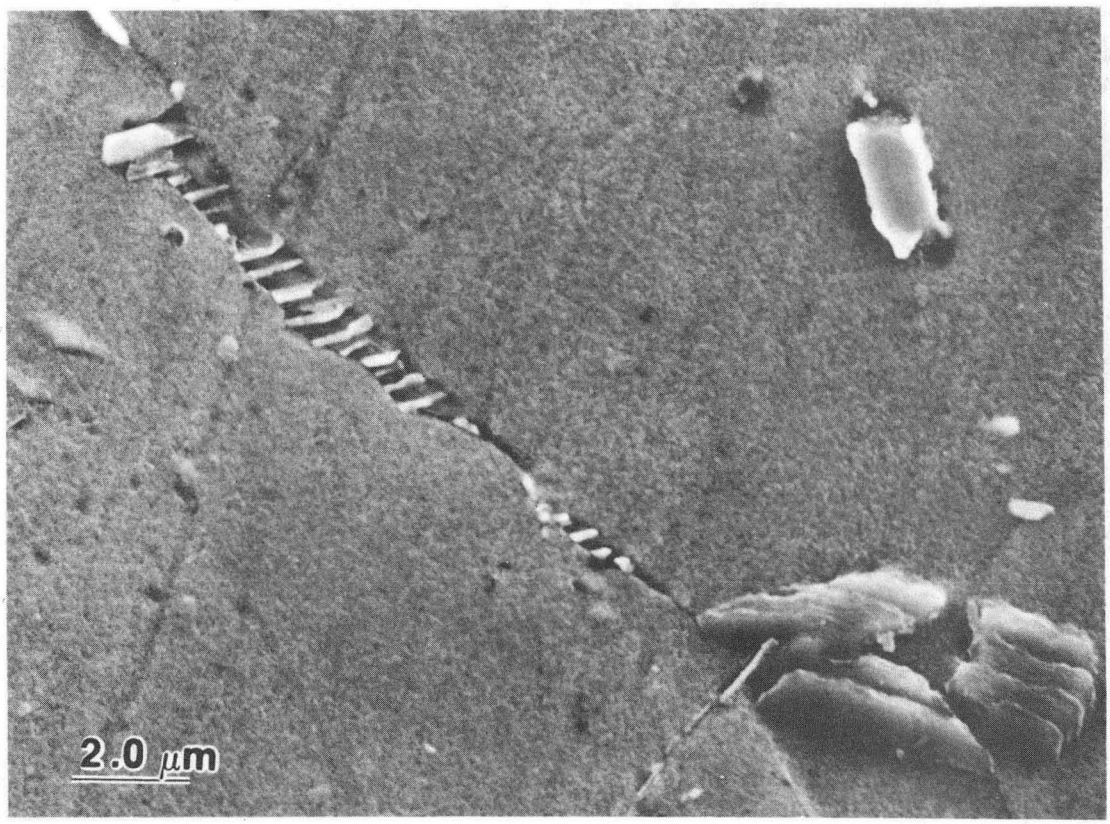

Figure 3a XBB 827-6440

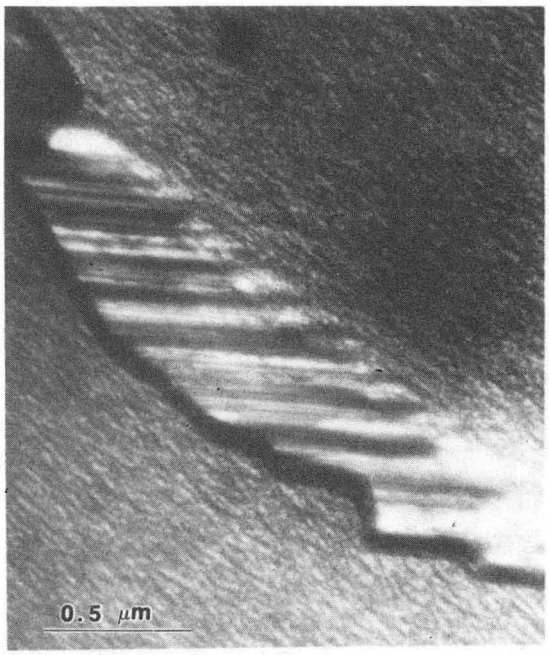

Figure 3b

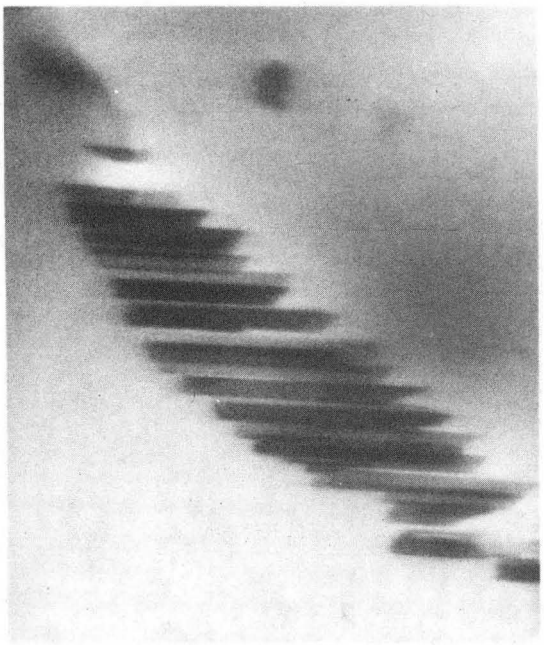

Figure 3c

XBB 827-6445

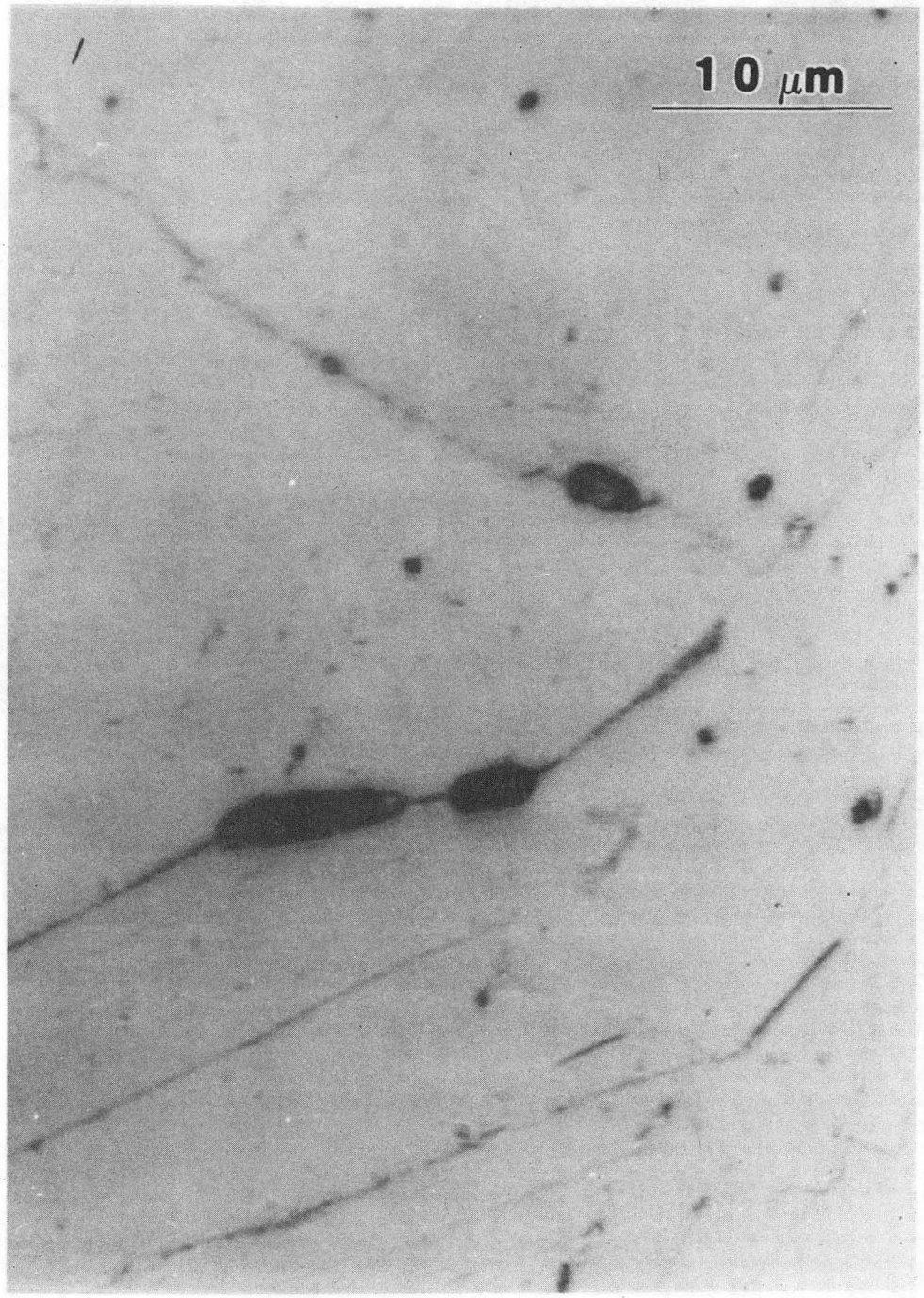

Figure 4 XBB 827-6444

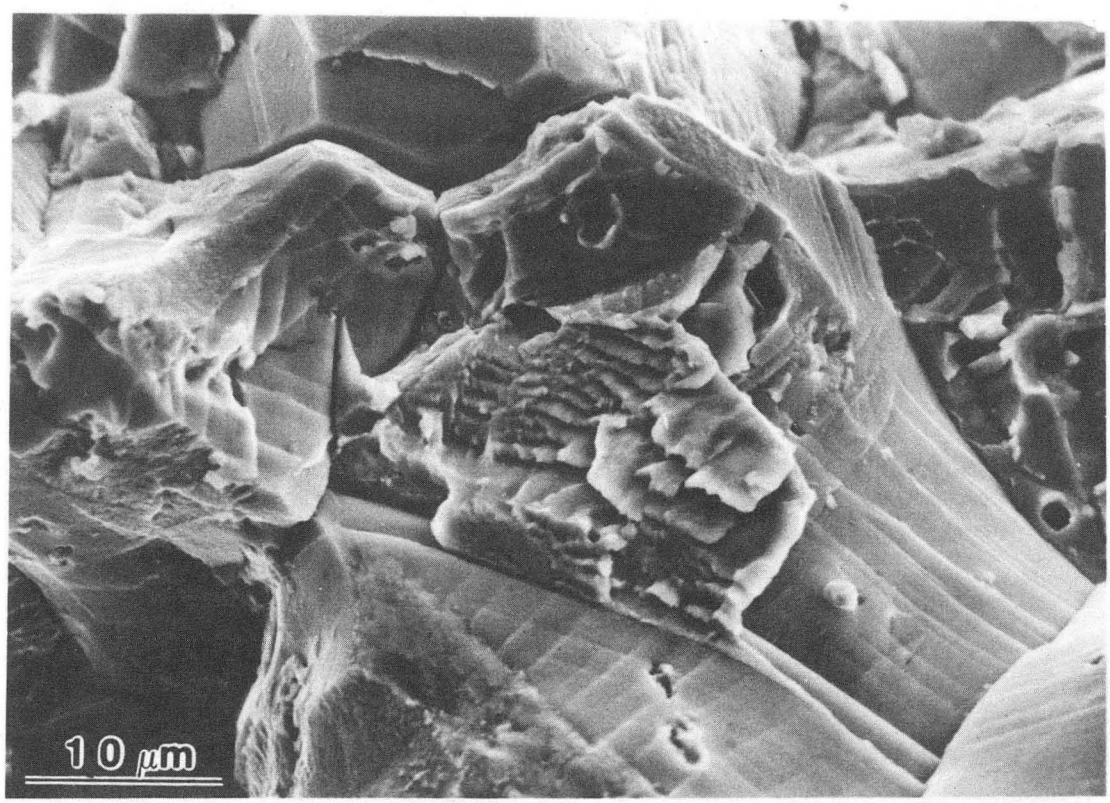

Figure 5 XBB 827-6443

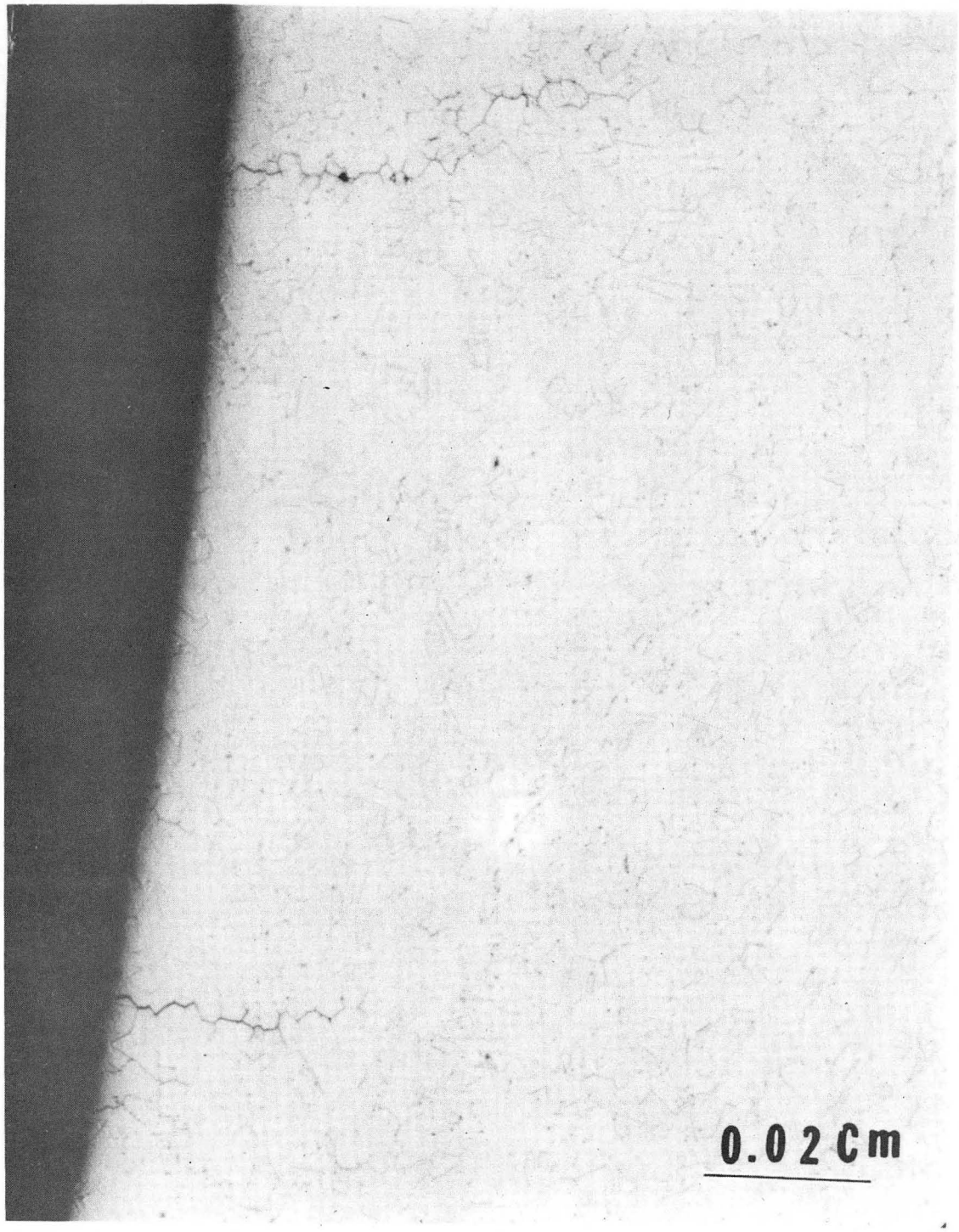

Figure 6

XBB 827-6442

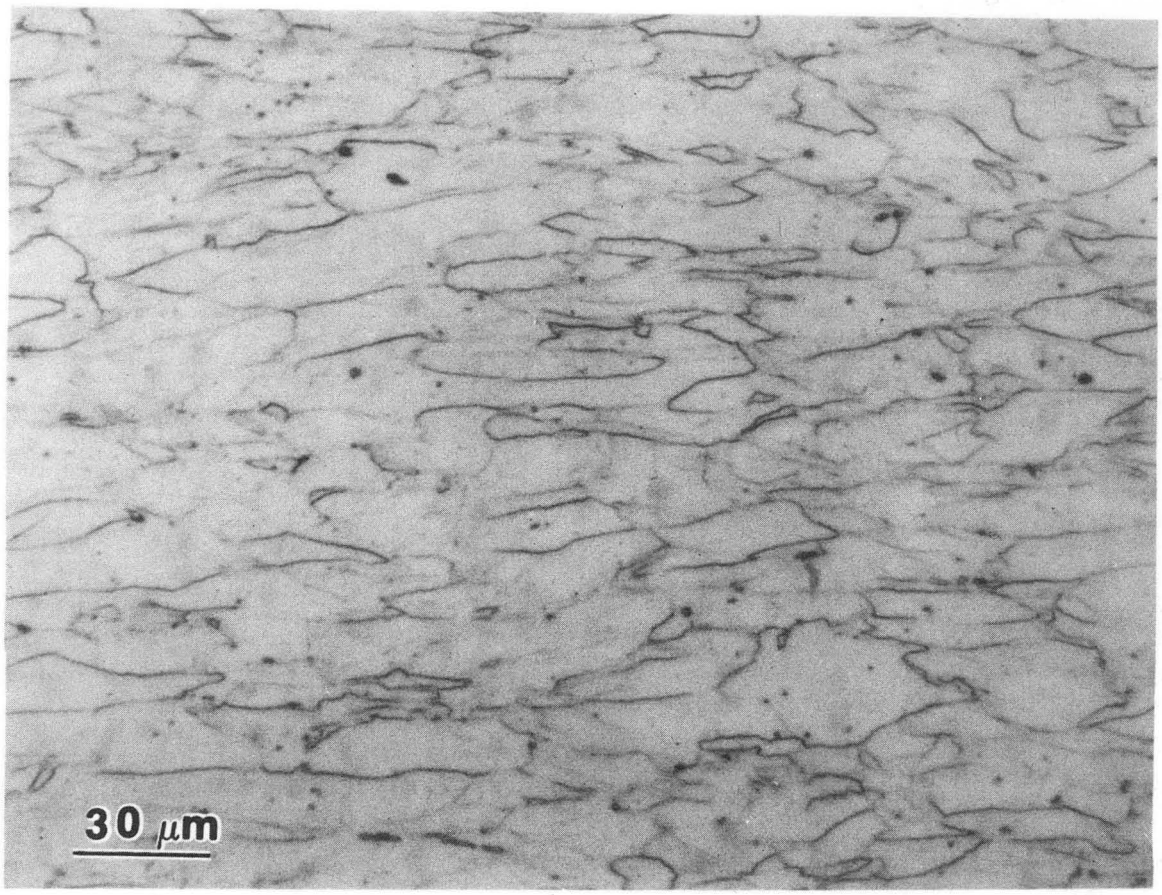

Figure 7

XBB 827-6452

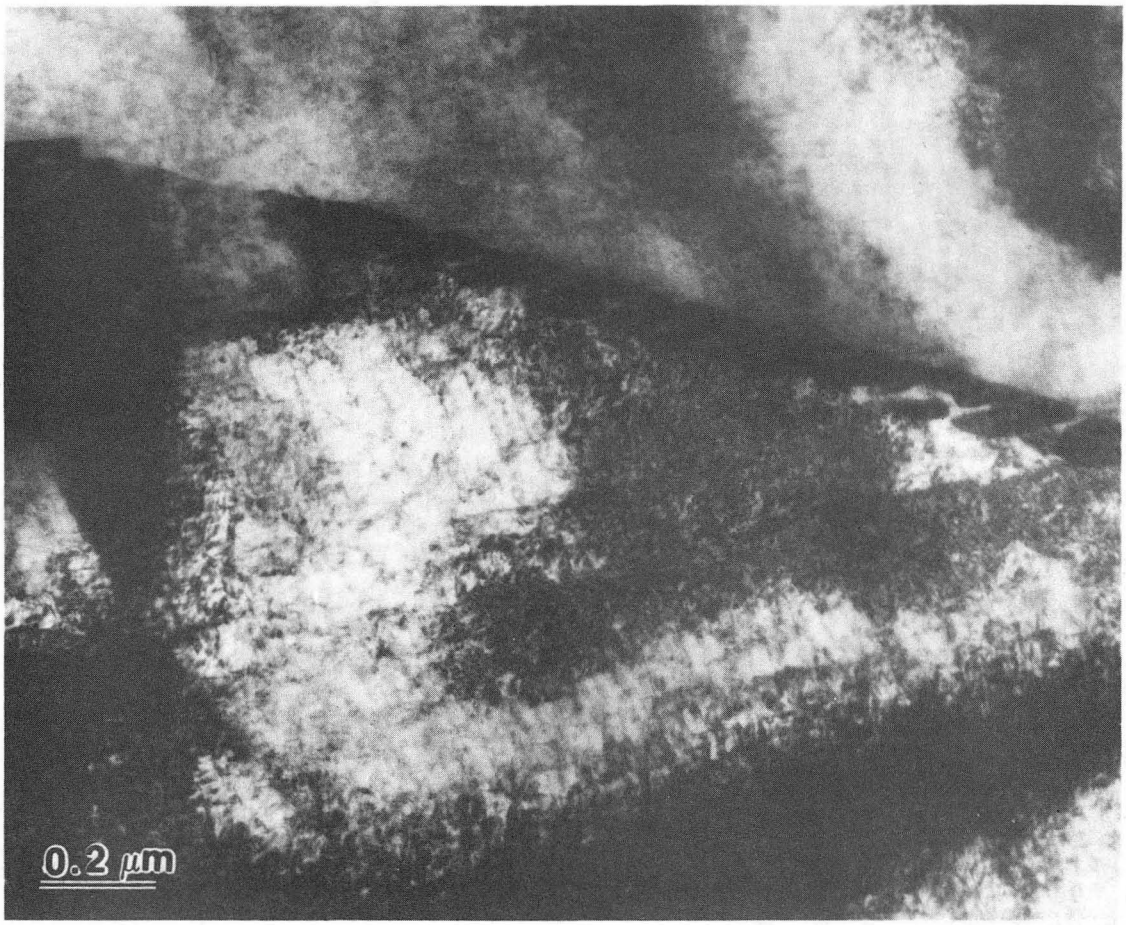

Figure 8

XBB 827-6451

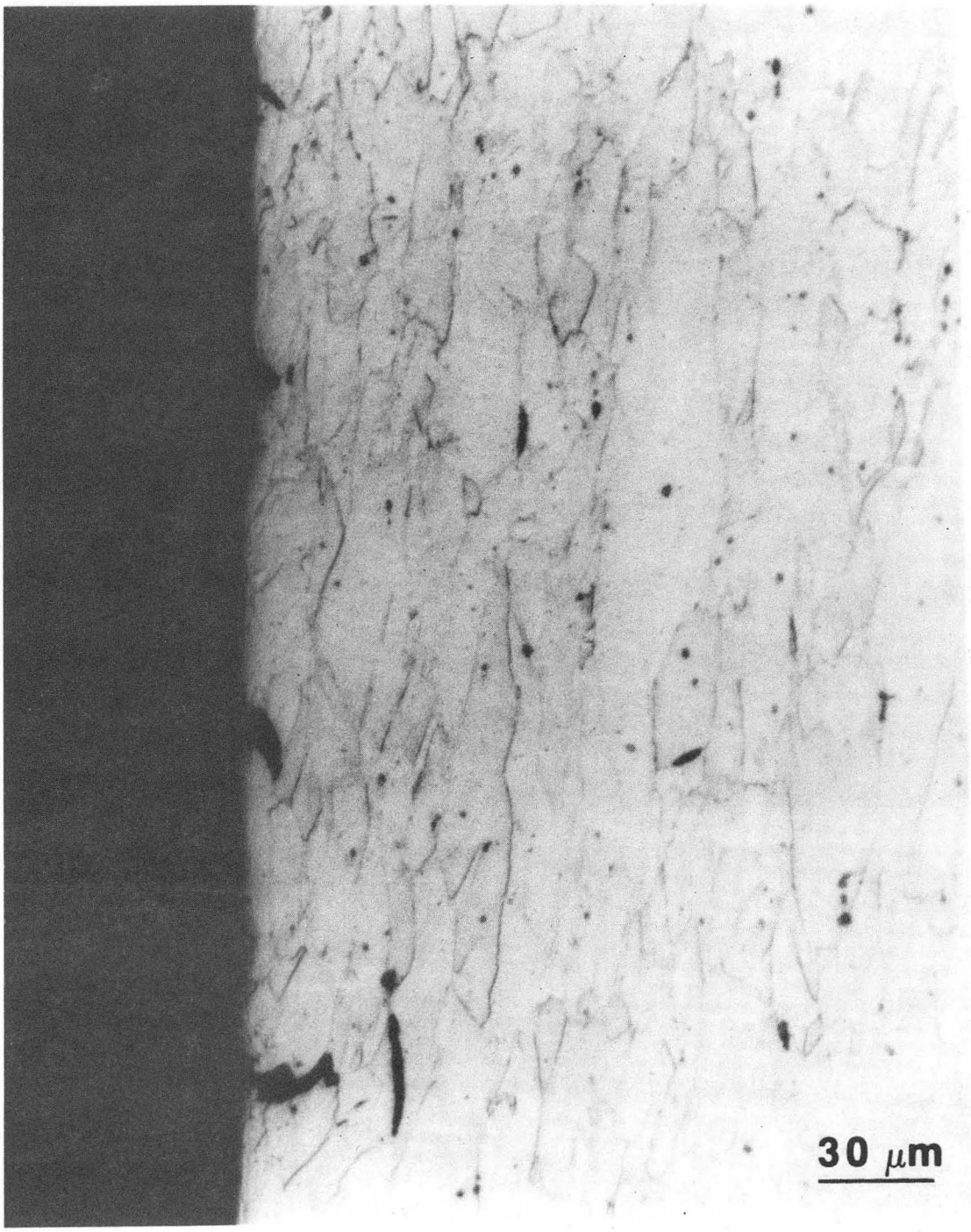

Figure 9

XBB 827-6450

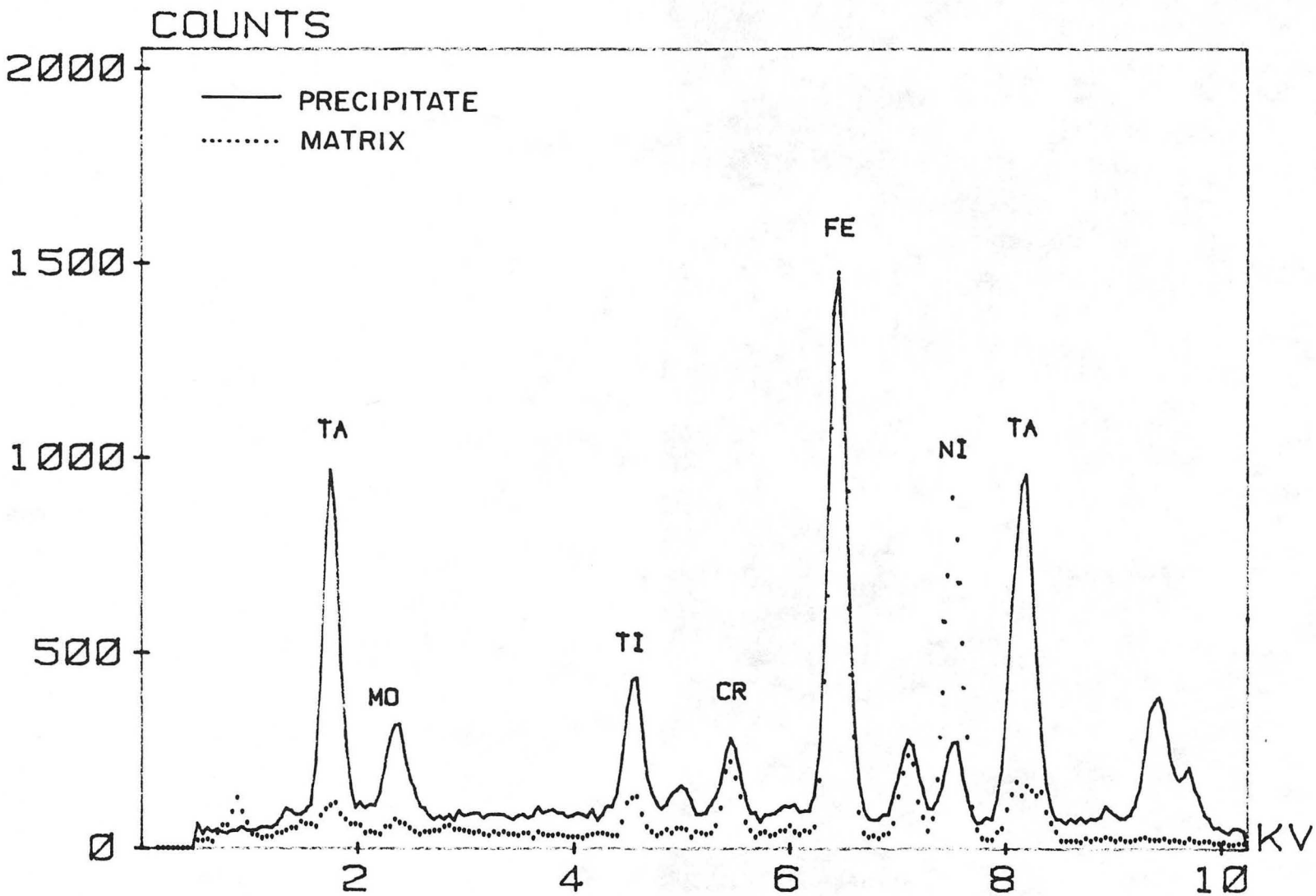

Figure 10

XBL827-6225

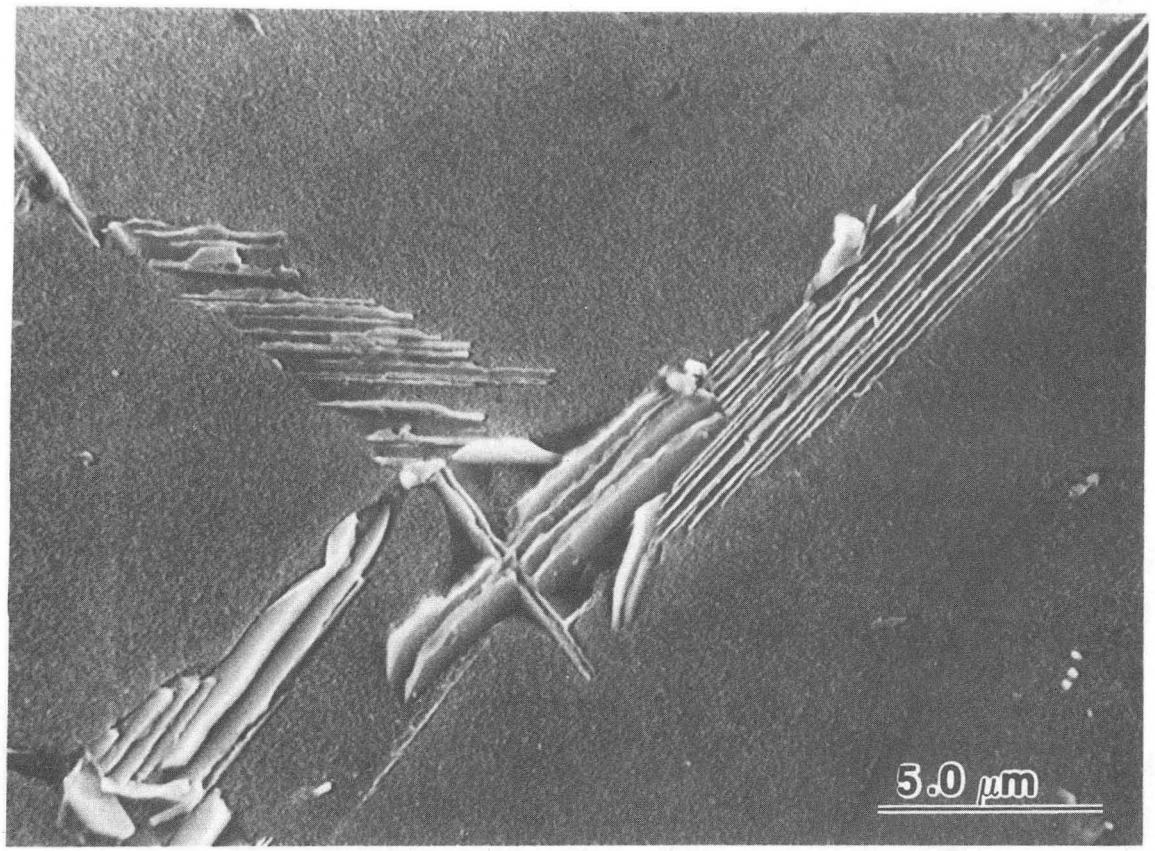

Figure 11

XBB 827-6449

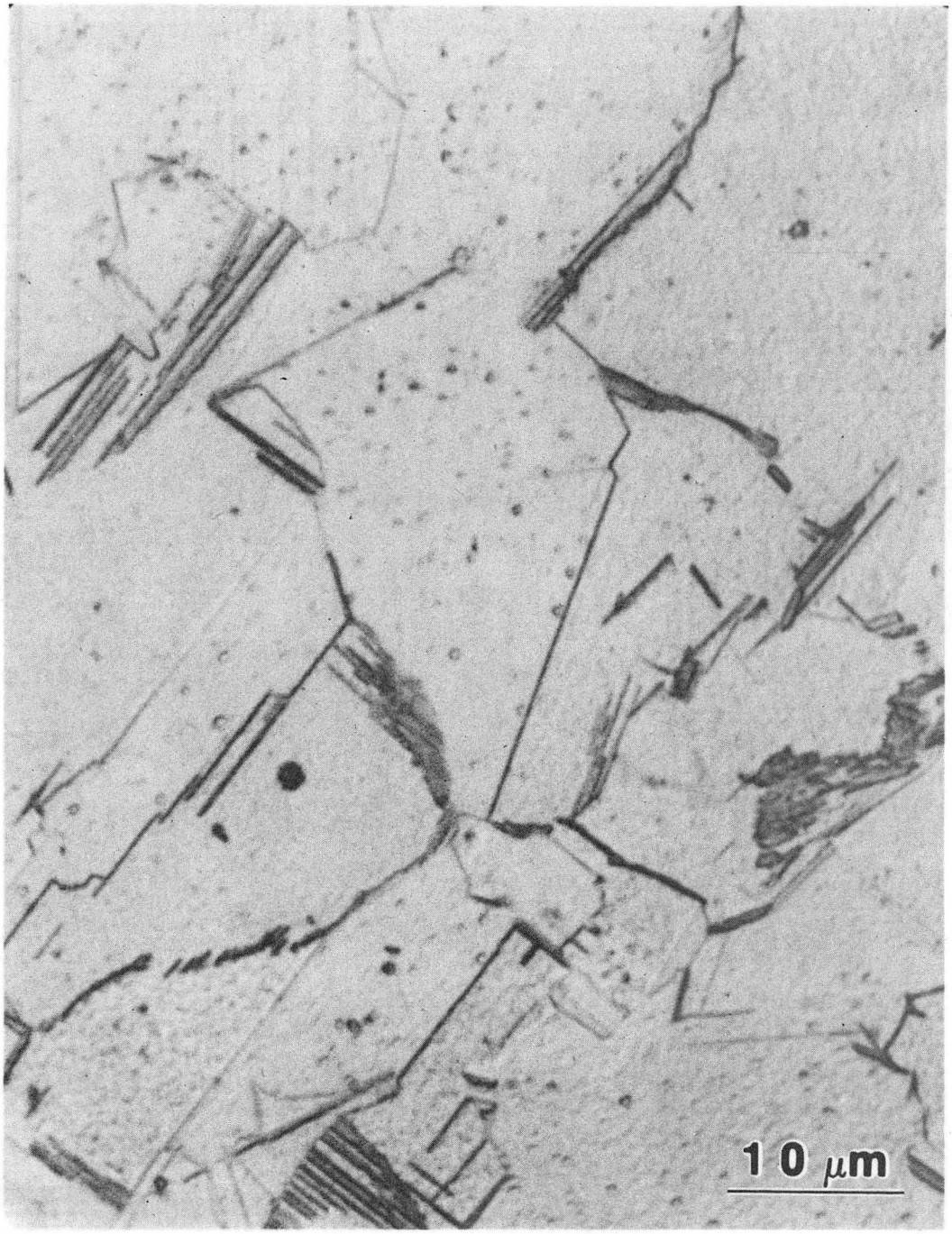

Figure 12 XBB 827-6448

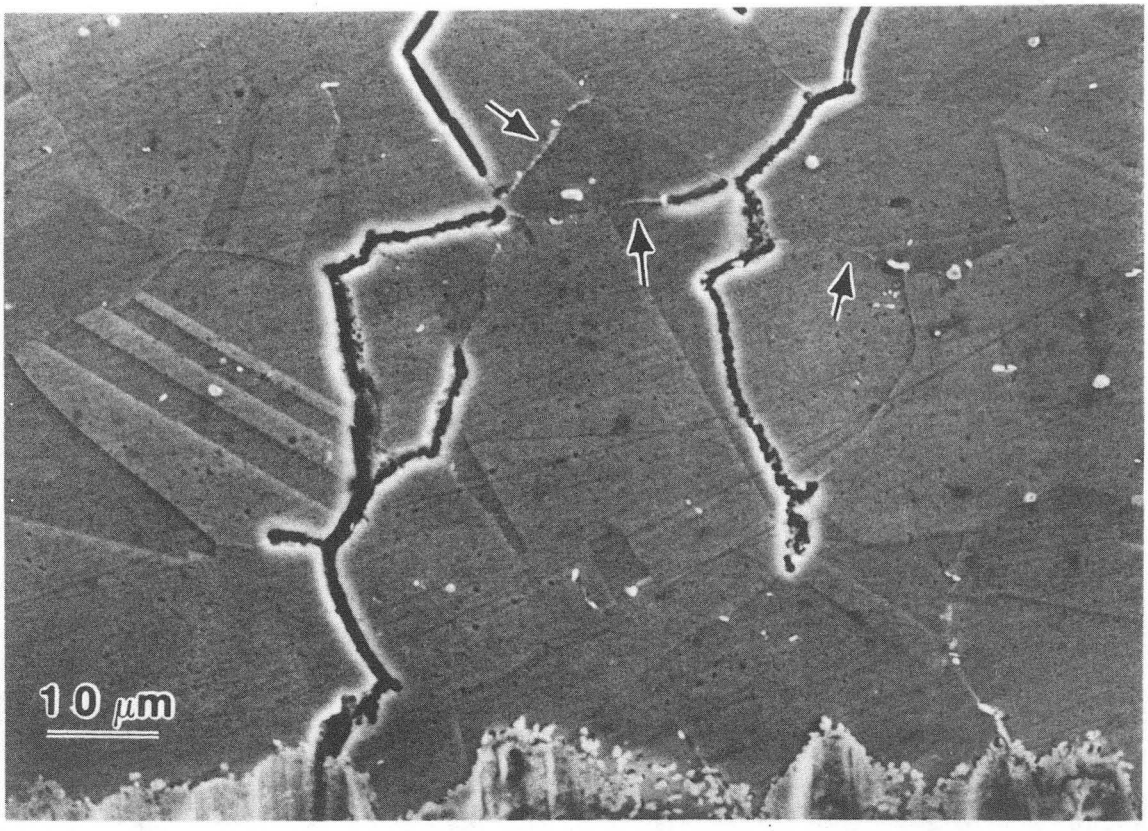

Figure 13

XBB 827-6447

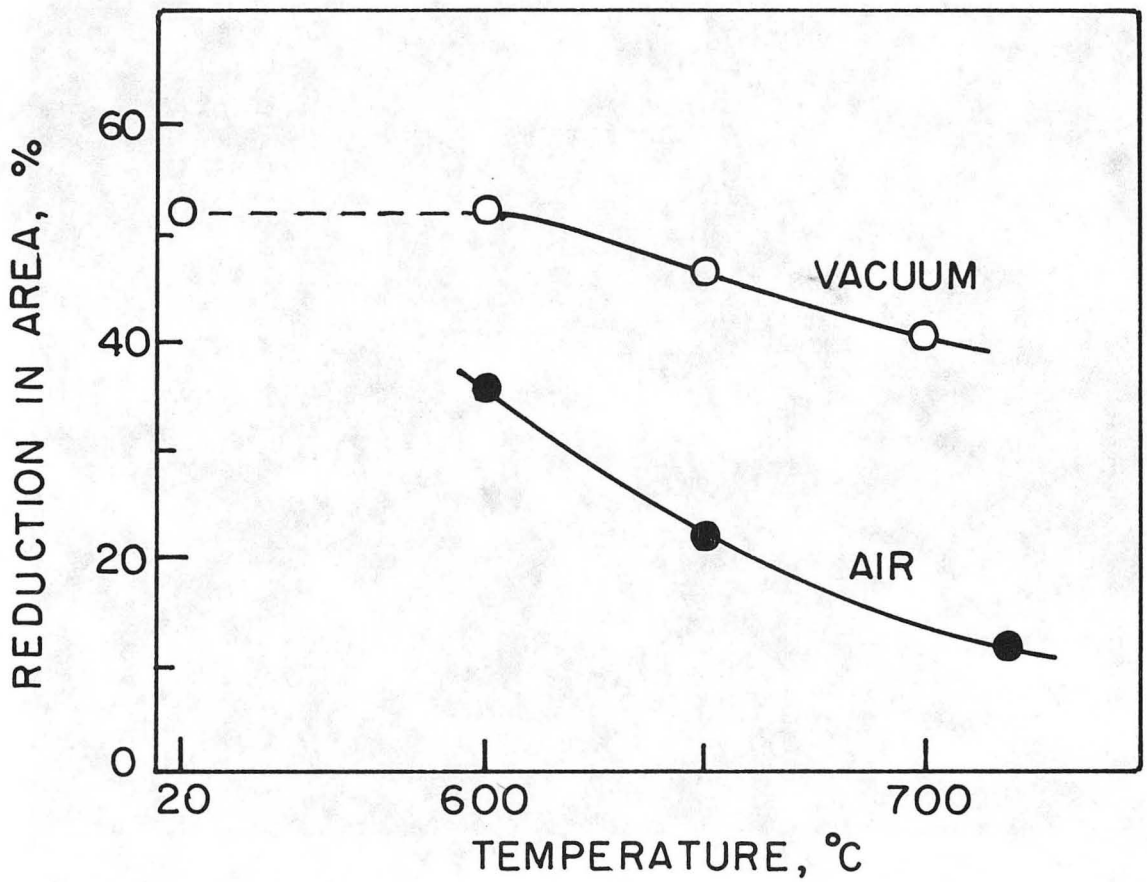

Figure 14

XBL 827-6224

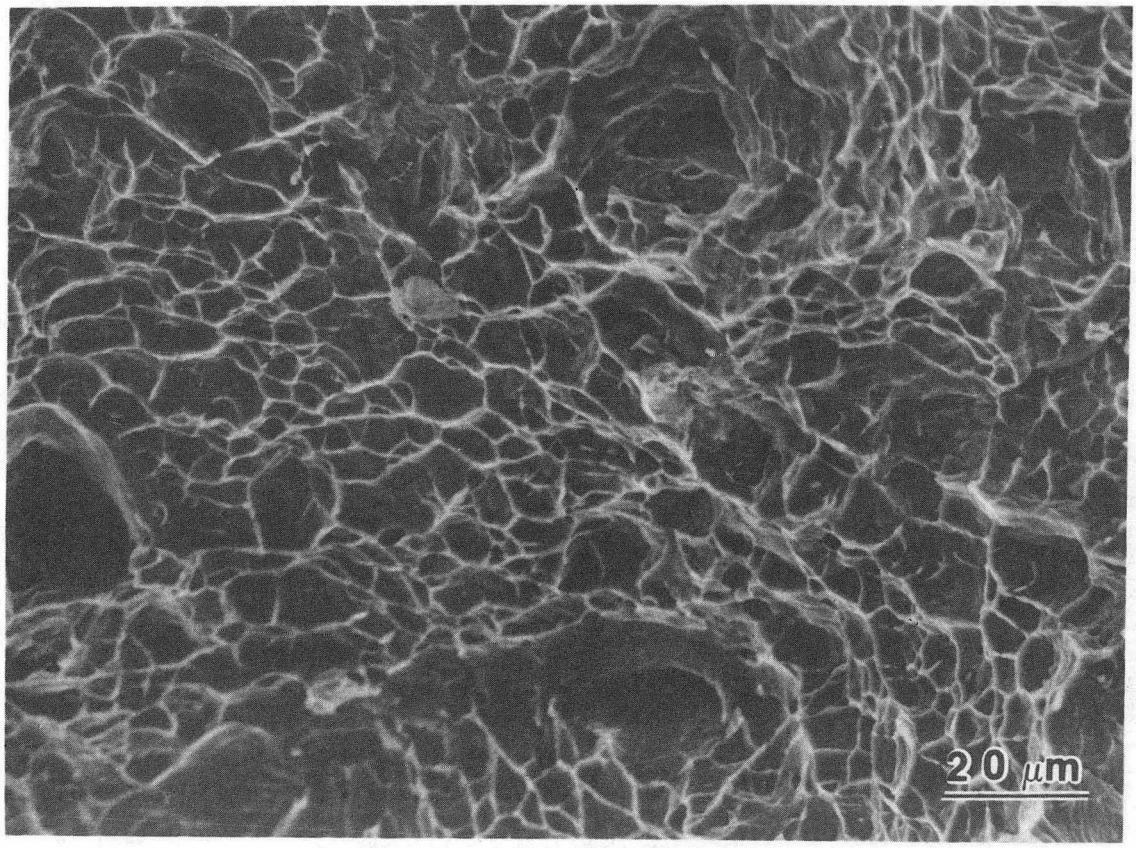

Figure 15

XBB 827-6446

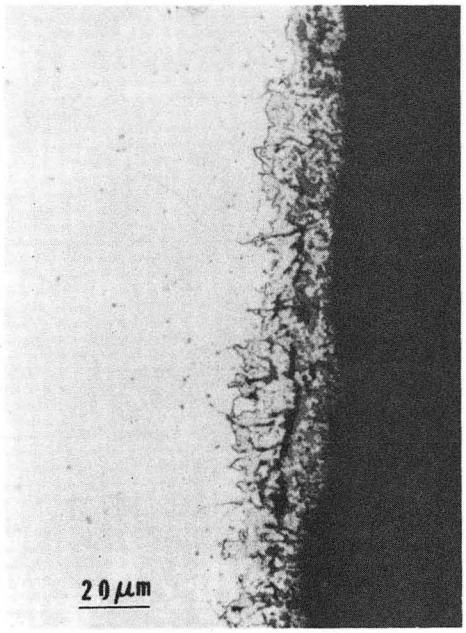

Figure 16a

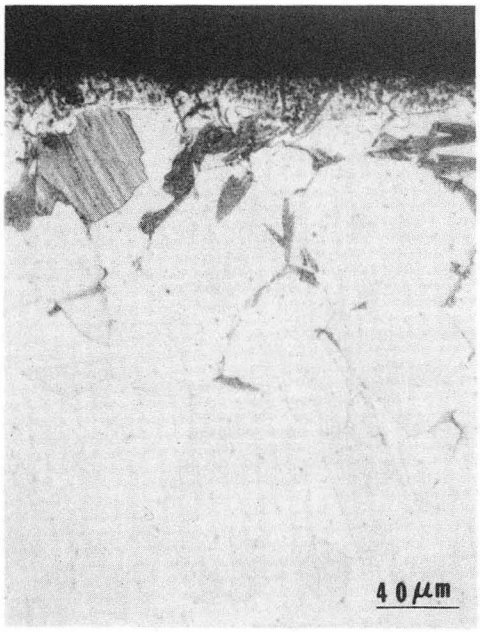

Figure 16b

XBB 827-6458

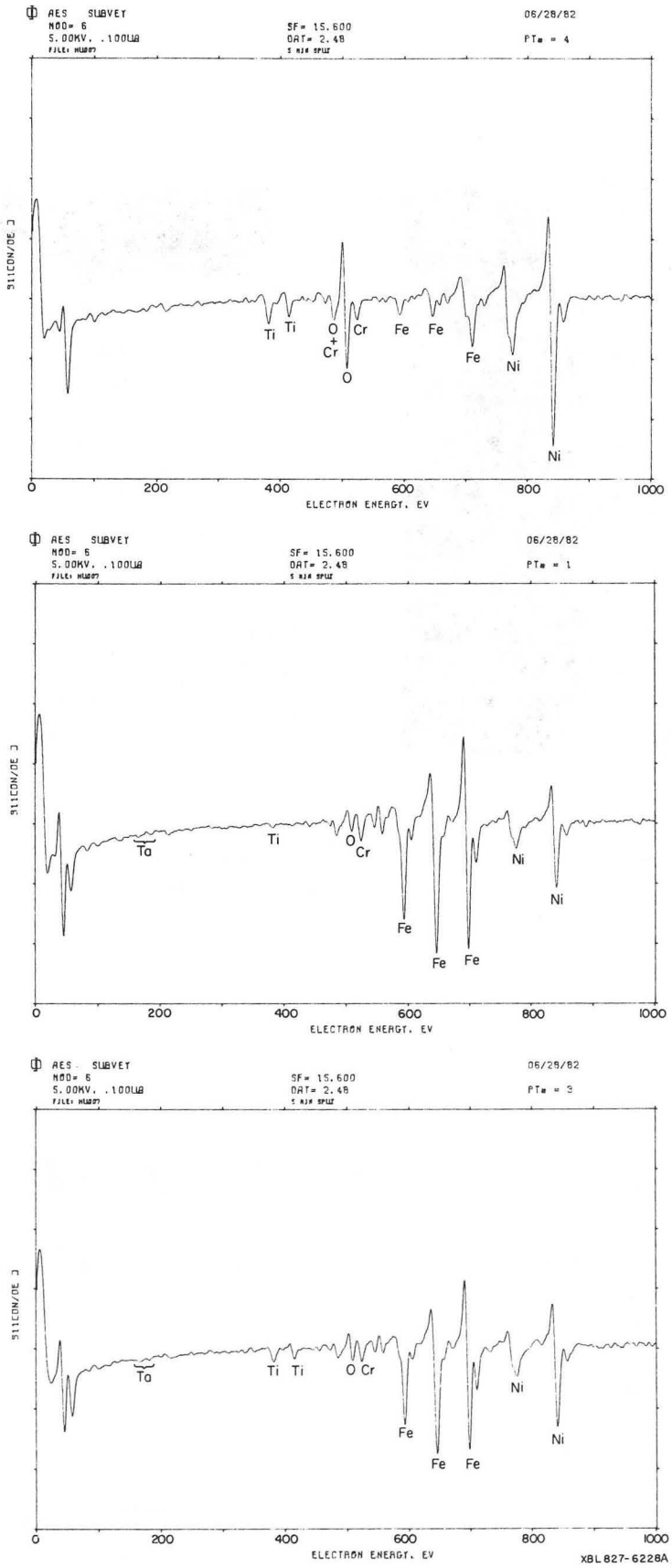
AES SUBVET
MOD= 6
5.00KV. .100UA
SF= 15.600
DAT= 2.48
06/28/82
PT# = 4
Ti
Ti
O
+
Cr
O
Cr
Fe
Fe
Fe
Ni
Ni
0
200
400
600
800
1000
ELECTRON ENERGY, EV
AES SUBVET
MOD= 6
5.00KV. .100UA
SF= 15.600
DAT= 2.48
06/28/82
PT# = 1
Ta
Ti
O
Cr
Fe
Fe
Fe
Ni
Ni
0
200
400
600
800
1000
ELECTRON ENERGY, EV
AES SUBVET
MOD= 6
5.00KV. .100UA
SF= 15.600
DAT= 2.48
06/28/82
PT# = 3
Ta
Ti
Ti
O
Cr
Fe
Fe
Fe
Ni
Ni
0
200
400
600
800
1000
ELECTRON ENERGY, EV
XBL 827-6228A

Figure 17

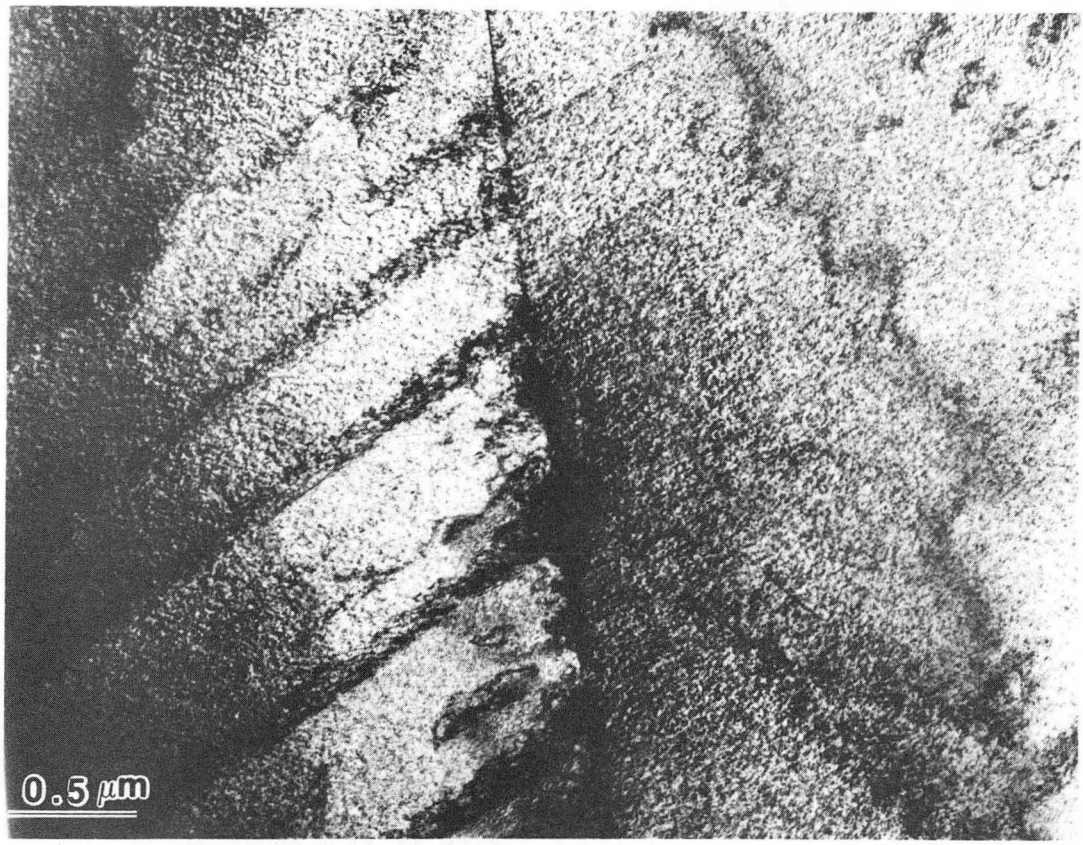

Figure 18

XBB 827-6457

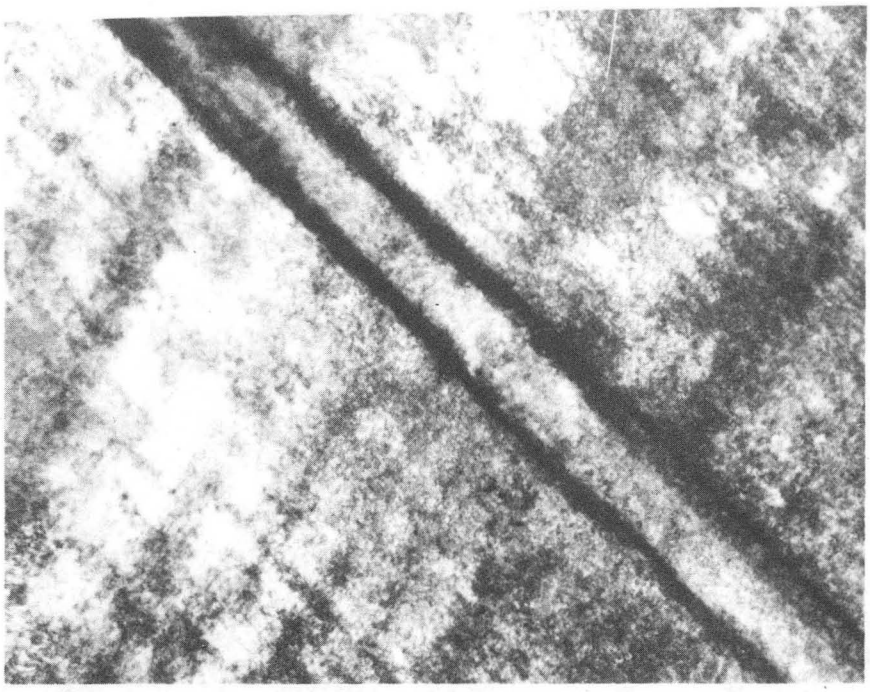

Figure 19a

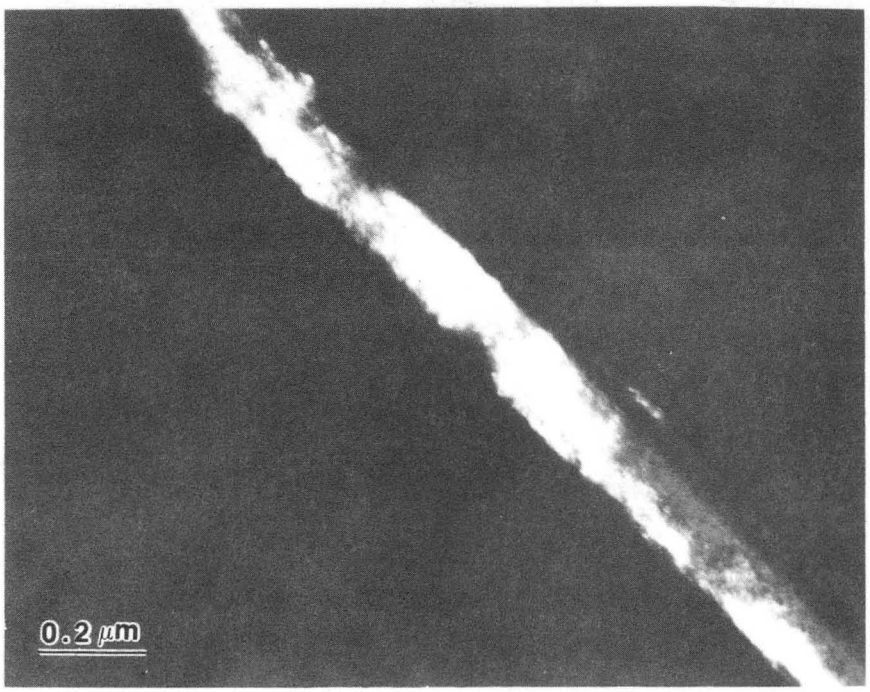

Figure 19b

XBB 827-6456

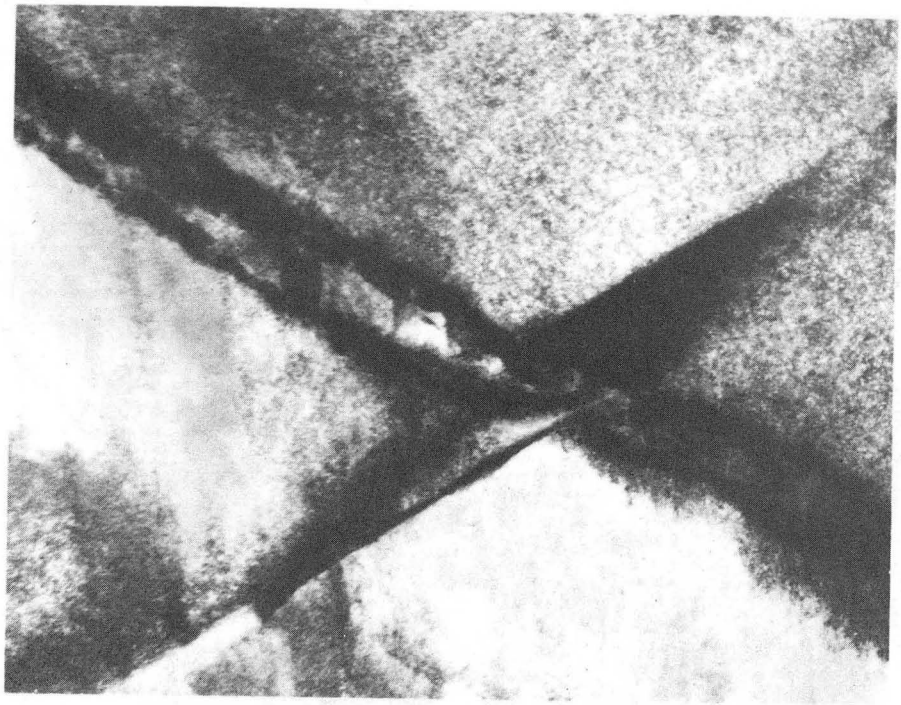

Figure 20a

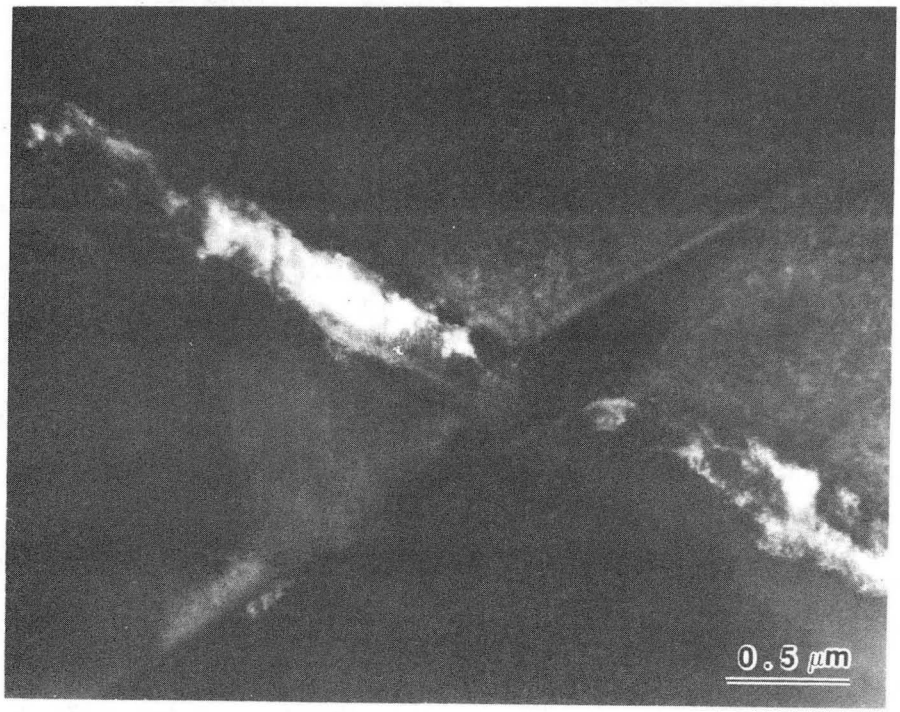

Figure 20b

XBB 827-6455

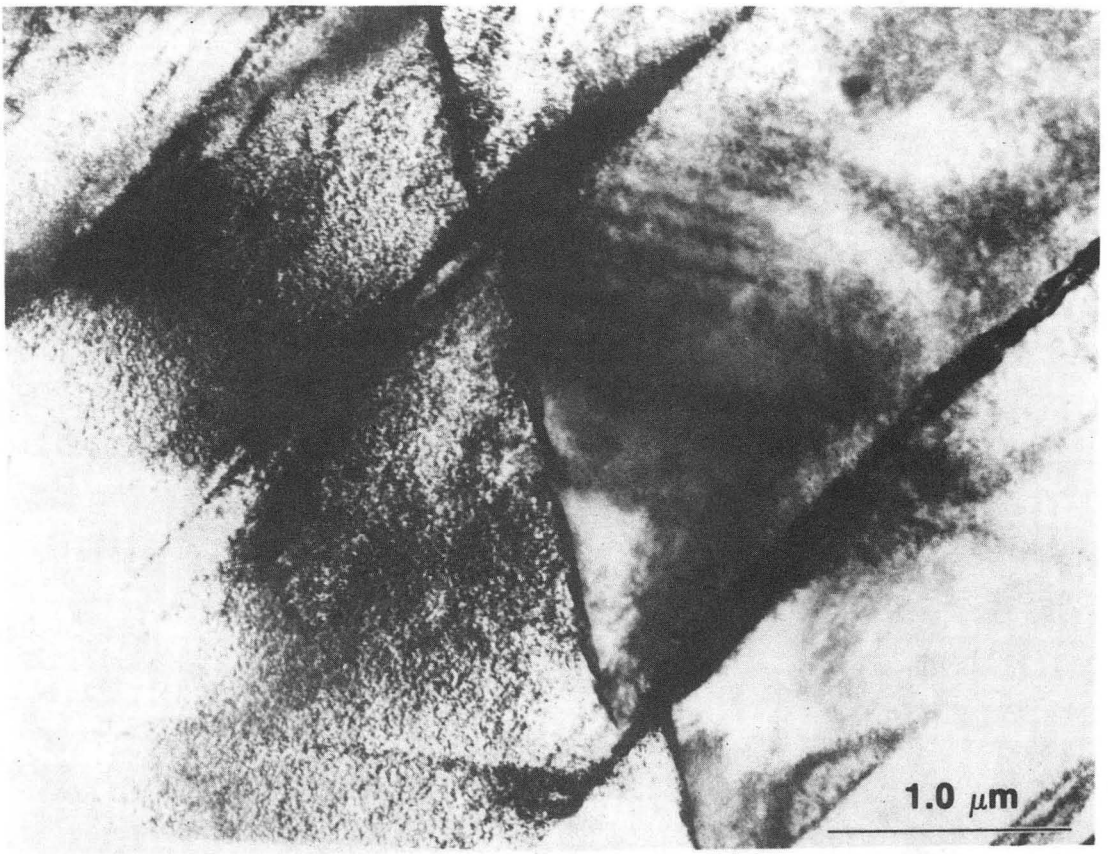

Figure 21 XBB 827-6454

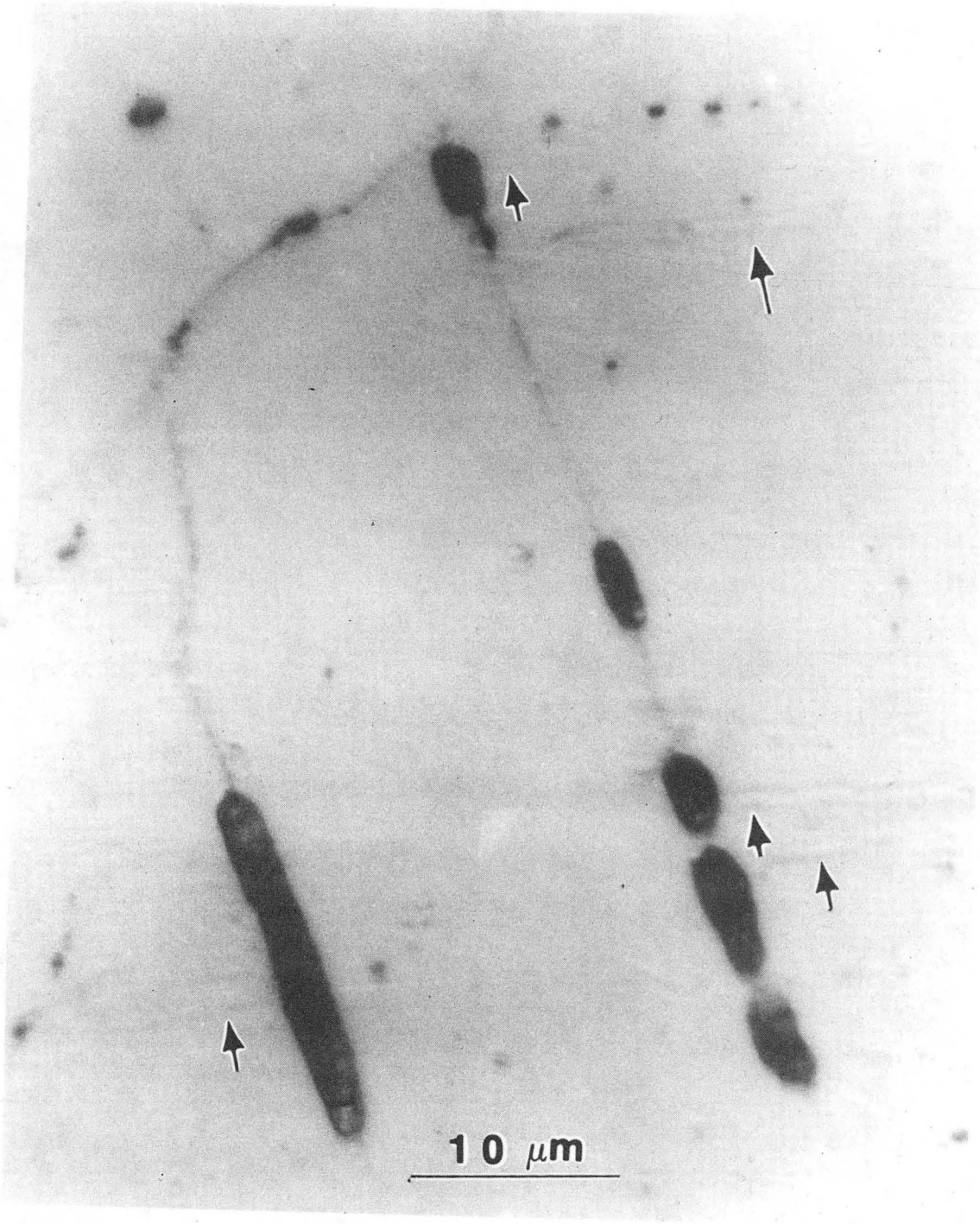

Figure 22

XBB 827-6453

This report was done with support from the Department of Energy. Any conclusions or opinions expressed in this report represent solely those of the author(s) and not necessarily those of The Regents of the University of California, the Lawrence Berkeley Laboratory or the Department of Energy.

Reference to a company or product name does not imply approval or recommendation of the product by the University of California or the U.S. Department of Energy to the exclusion of others that may be suitable.

TECHNICAL INFORMATION DEPARTMENT
LAWRENCE BERKELEY LABORATORY
UNIVERSITY OF CALIFORNIA
BERKELEY, CALIFORNIA 94720